A Framework for Extrusion Screw Design

Amanda Mile and Emma Frick

DIVISION OF INNOVATION | DEPARTMENT OF DESIGN SCIENCES
FACULTY OF ENGINEERING LTH | LUND UNIVERSITY
2026

MASTER THESIS

A Framework for Extrusion Screw Design

Degree Project in Product Development

Amanda Mile and Emma Frick

LUND UNIVERSITY

A Framework for Extrusion Screw Design

Degree Project in Product Development

Published by
Department of Design Sciences
Faculty of Engineering LTH, Lund University
P.O. Box 118, SE-221 00 Lund, Sweden

Subject: Product Development (MMKM05)
Division: Division of Innovation Engineering, Department of Design Sciences, Faculty of Engineering LTH, Lund University
Supervisor: Axel Nordin (LTH) and Peter Vighagen (Tetra Pak)
Co-supervisor: RenanMelhado Mazza
Examiner: Joze Tavcar

Abstract

This thesis presents the development of a structured framework for extrusion screw design based on geometrical parameters, with the aim of improving understanding and supporting design decisions in industrial extrusion processes. The work was carried out in collaboration with Tetra Pak and focuses on the extrusion system used in injection compression molding of Tetra Top lids.

An initial numerical simulation approach was explored, but due to limitations related to model stability and setup complexity, the study proceeded using an analytical modelling approach. The analytical models were used to describe the relationship between screw geometry and process performance, focusing on mass flow rate and power consumption in the metering section. The models were evaluated and compared with existing experimental data, showing that they capture the overall behaviour of the process, although with some deviations in absolute values.

To systematically analyse the influence of geometrical parameters, a Design of Experiments approach was applied. Response surface models were developed to represent the relationships between input and output parameters, enabling further analysis of parameter trends, parameter influence and trade-offs. The results show that most geometrical parameters influence mass flow rate and power consumption in opposite directions, highlighting a clear trade-off between high throughput and low energy consumption. Additionally, only a few parameters dominate the overall behaviour, which is important for practical design decisions.

Based on these results, a structured framework for extrusion screw design was proposed. The framework provides a systematic approach for analysing parameter trends, evaluating their influence, and handling trade-offs between different design objectives. It can be applied to processes similar to the studied case and serves as a decision support tool for screw design.

Overall, the study demonstrates how a model-based approach can support extrusion screw design and improve understanding of the relationship between screw geometry and process performance.

Keywords: Injection compression molding, extrusion screw design, design of experiments, response surface, mass flow rate, power consumption

Sammanfattning

Denna studie presenterar utvecklingen av ett ramverk för design av extruderskruvar baserat på geometriska parametrar, med syftet att öka förståelsen och stödja designbeslut i industriella extruderingsprocesser. Arbetet genomfördes i samarbete med Tetra Pak och fokuserar på extruderingssystemet som används vid kompressionsformsprutning av Tetra Top.

Till en början undersöktes en numerisk simuleringslösning, men på grund av begränsningar kopplade till modellstabilitet och komplexitet i uppsättning, fortsatte studien med en analytisk modell istället. De analytiska modellerna användes för att beskriva sambandet mellan skruvgeometri och processprestanda, med fokus på massflöde och energiförbrukning i sista delen av skruven. Modellerna utvärderades och jämfördes med befintlig experimentell data, vilket visade att de fångar processens övergripande beteende, även om avvikelser i absoluta värden förekommer.

För att systematiskt analysera påverkan från geometriska parametrar användes Design of Experiments. Respons surface-modeller utvecklades för att representera sambanden mellan in- och utparametrar, vilket möjliggjorde vidare analys av parametertrender, parameterpåverkan och avvägningar mellan olika mål. Resultaten visar att de flesta geometriska parametrar påverkar massflöde och energiförbrukning i motsatta riktningar, vilket visar på att det krävs en avvägning mellan högt massflöde och låg energiförbrukning. Dessutom dominerar endast ett fåtal parametrar det övergripande beteendet, vilket är viktigt ur ett praktiskt designperspektiv.

Baserat på dessa resultat föreslogs ett strukturerat ramverk för design av extruderskruvar. Ramverket ger en systematisk metod för att analysera parametertrender, utvärdera deras påverkan samt hantera avvägningar mellan olika designmål. Det kan tillämpas på processer som liknar den studerade och kan fungera som ett beslutsstöd vid skruvdesign.

Sammanfattningsvis visar studien hur en modellbaserad metod kan stödja design av extruderskruvar och öka förståelsen för sambandet mellan skruvgeometri och processprestanda.

Nyckelord: kompressionsformsprutning, extruderingsskruvsdesign, Design of Experiments, Response surface, massflöde, effektförbrukning

Acknowledgments

First, we would like to thank Tetra Pak for the opportunity to carry out this thesis and for the support we have received through the projcet. We would especially like to thank our supervisor Peter Vighagen for the guidance and feedback throughout the project, as well as RenanMelhado Mazza for valuable support. We would also like to thank Henrik Holm, Patrik Månsson, Viktor Petersson and Elin Persson Jutemar for their valuable input and support during the work. Their insights and willingness to share knowledge have been highly appreciated.

Finally, we would also like to thank our supervisor from LTH, Axel Nordin. Your support and guidance throughout the project have been greatly appreciated. We would also like to thank our examiner Joze Tavcar.

Lund, May 2026

Amanda Mile & Emma Frick

Table of Content

Appendices

List of acronyms and abbreviations

BBD	Box-Behnken Design
CCD	Central Composite Design
DOE	Design of Experiment
GM	Granulate Mix
HDPE	High Density Polyethylene
LFU	Lid Forming Unit
SDG	Sustainable Development Goal

1 Introduction

This chapter introduces the thesis project including a short introduction of Tetra Pak, as well as the background and context that motivate this research. It highlights the current solution, its challenges and possible areas of improvement. Additionally, the mission statement, delimitations and clarification of confidentiality and decision making are established. Finally, this chapter presents the thesis' relevance to sustainable development, ethical considerations as well as an overview of the thesis structure.

1.1 About Tetra Pak

Tetra Pak is a leading food processing and packaging solutions company specializing in primarily liquid food products like milk and juices as well as sauces and soups. The company commits to making food safe and available everywhere by protecting the food, people and planet. Tetra Pak is known for its innovative packaging designs, including the original tetrahedral shape, and offers various packaging solutions such as Tetra Brik, Tetra Prisma and Tetra Top. This thesis will focus on Tetra Top filling machines and its correlating equipment.

1.2 Background

This thesis was carried out in cooperation with the D&T Packaging Equipment & Automation Department at Tetra Pak Packaging Solutions AB in Lund. The department specializes in optimizing processes and equipment related to Tetra Top filling machines. The Tetra Pak team provided support, insights and expertise from technology specialists throughout the project.

In injection-compression molding, the extrusion screw plays a critical role in achieving the desired efficiency and melt quality. Even minor modifications to the screw geometry can significantly influence pellet melting behavior and, consequently, the overall process performance. The extrusion screws currently used in Tetra Top filling machines are supplied by external manufacturers, and the internal development teams at Tetra Pak have limited insight into the detailed design and functional rationale behind these geometries. Tetra Pak wishes to have a better in house understanding of the extrusion screws in the future, therefore it is essential to establish a clear understanding of the key design parameters and their effects on process outcomes. Therefore, this thesis contributes to the development of a structured framework to support the selection and design of appropriate screw geometries for Tetra Paks extrusion processes.

1.2.1 The principle of Tetra Top Lid Forming Unit

The current Lid Forming Unit (LFU) has the purpose to mold plastic lids to paper sleeves. This creates packages that has a lower part in paper board and an upper part made of plastic, the package Tetra Top is seen in Figure 1.1. The filling machine produces four packages at the same time using two extruders, which means that one extruder has to be able to process material for two packages each cycle. In the current filling machine the granulate mix (GM) is inserted into the hopper, and thereafter led into the extruder where the processing of the material begins. When the plastic is melted and processed properly the melt is transported from the extruder to an accumulator, see Figure 1.2. The accumulator regulates the screw's rotational speed, depending on the amount of melted material in the accumulator. Because of this the extruder is always processing material, and usually never stands still. From the accumulator the material is led via heating hoses to the hot channels, and then transported into the mold.

Figure 1.1: Tetra Pak's shape Tetra Top [1].

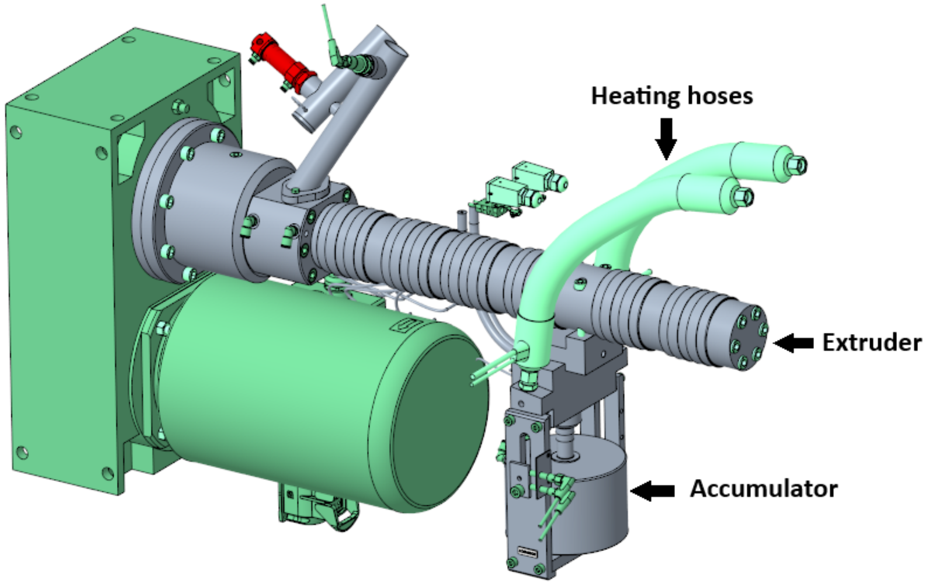

Figure 1.2: Assembly of extruder, heating hoses and accumulator in the LFU.

1.3 Mission Statement

The main objective for this thesis is to develop a structured framework for extrusion screw optimization, focusing on geometrical parameters to increase mass flow and optimize process parameters such as energy consumption. The project will explore how variations in screw geometry, such as length, diameter, channel depth and pitch, affect mass flow rate and power consumption. The framework aims to guide Tetra Pak when deciding on which extrusion screw to use depending on desired process goals.

1.4 Delimitations

The scope of this thesis is limited to ensure a focused and feasible study. The following delimitations apply:

- Only one material is considered, high density polyethylene (HDPE).
- The study focuses exclusively on geometrical parameters, while process parameters are kept constant.

- The screw geometry must comply with existing dimensional constraints and fit within the current LFU.
- The analysis is limited to the metering section of the extrusion screw.
- Verification is limited to comparison with existing experimental data, and no new physical testing or prototyping is performed.
- The study focuses only on the screw and not the barrel, although the clearance between screw and barrel is studied.

1.5 Confidentiality Notice

Due to Tetra Pak's confidentiality standards, sensitive information presented in this report has been generalized or anonymized throughout the report. The following section outlines and clarifies the key material that has been restricted or modified in accordance with these confidentiality requirements.

- The precise geometry, measures and tolerances of extrusion screw and barrel has been erased from the results.
- The material specification for the granulate mix used in Tetra Top will be referred to as GM, and not specified further.
- Specific process parameters will not be specified.
- Drawings and CAD files for the LFU and the extruder are used but not included in this report.
- Photographs of existing extrusion screws and other equipment used within Tetra Pak's facilities are either excluded or replaced with manually created illustrations to avoid exposing internal designs.

1.6 Clarification on Decision Making

Throughout this thesis work, all tasks, analyses, and decisions were initiated, executed, and evaluated by the two students, unless explicitly stated otherwise. While supervisors provided guidance and feedback, the overall planning, methodological choices, and implementation of the work were independently carried out by the students.

1.7 Relevance for Sustainable Development

The development of a structured design approach for extrusion screw optimization contributes to sustainable development in several ways. By improving the extrusion screw geometry to enhance process performance, the overall energy consumption during extrusion could be reduced. Since extrusion is an energy intensive process, even marginal improvements can lead to significant reductions in operational energy use over time, supporting Sustainable Development Goal (SDG) 12 (Responsible Consumption and Production)[2].

Using a structured design methodology instead of relying on extensive physical testing reduces consumption of polymer and paperboard during development and offers a repeatable, data driven path to identifying an optimal screw configuration without iterative trial and error experiments. By balancing performance improvements with cost efficiency, the methodology supports sustainable decision making, enabling cost effective screws that maintain high processing performance and reduce maintenance needs. Together, these benefits minimize resource use across the equipment life cycle and align with sustainable manufacturing principles and the goals of SDG 9 (Industry, Innovation and Infrastructure)[3].

Finally, by providing Tetra Pak with a systematic framework for selecting or designing extrusion screws based on desired output, the thesis supports informed and transparent engineering decisions. This facilitates future in house screw development that can be aligned with broader environmental targets, including energy reduction, resource efficiency, and improved recyclability of materials.

1.8 Ethical Considerations

This project does not involve human participants, and no personal data is collected. The ethical considerations therefore relate primarily to how the project's outcome and methods influence Tetra Pak as an organization and how confidential information is handled. The project delivers a structured method for extrusion screw optimization that can reduce material use, testing and development costs. Since the project does not negatively impact individuals and contributes to a more resource efficient development, this thesis project is considered ethically justified.

1.9 Outline of the Thesis

The report is divided into six main sections, each addressing a specific part of the study.

Chapter 1 introduces the background of the project, including objective, scope, and delimitations.

Chapter 2 presents the methodology based on the Double Diamond model. It includes the Discover, Define, Develop, and Deliver phases.

Chapter 3 covers the Discover phase of the project where the theoretical background is presented.

Chapter 4 presents the Define phase where parameters were selected, and constraints and parameter intervals were defined.

Chapter 5 includes the Develop phase where the simulation model and the analytical models were further developed and verified to experimental tests. A parameterized CAD model was also developed here, and a Design of Experiments were conducted in Minitab for response surface analysis and response optimization.

Chapter 6 covers the Deliver phase, and here the results from the Develop phase are presented.

Chapter 7 presents the final results which is the frameworks obtained from the Deliver phase as well as the optimized extrusion screw.

Chapter 8 covers an overall discussion of the project, addressing the study's objectives, limitations and sources of error.

Chapter 9 concludes the thesis by summarizing the main findings.

Finally, the report concludes with Appendix A where the work distribution and time plan are presented.

2 Methodology

This chapter presents the methodology used in the project. The work is structured according to the Double Diamond model, where each phase describes how the problem is explored, defined and analysed, and how the results are applied in the study. The chapter explains how the different phases have been used and how they form the basis for the analysis and results.

2.1 Double Diamond Model

The Double Diamond design process is a structured framework for innovation, developed by the Design Council. The model consists of two diamonds representing the process of exploring a problem more widely and deeply, divergent thinking, and then taking focused action, convergent thinking, see Figure 2.1. The first diamond covers the Discover phase as well as the Define phase. The Discover phase (Diverge) aims to develop an understanding of the problem by gathering insights through research, understanding needs, behaviors, and context. These insights can be used to define the challenge in a different way in the Define phase (Converge). The second diamond consists of the Develop phase, where many potential ideas are generated, and the Deliver phase, where the best solution is selected. In the Deliver phase, the solution is refined and tested until the final product is ready for implementation. The Double Diamond model encourages a proper breakdown of the problem and supports evidence-based decision making [4].

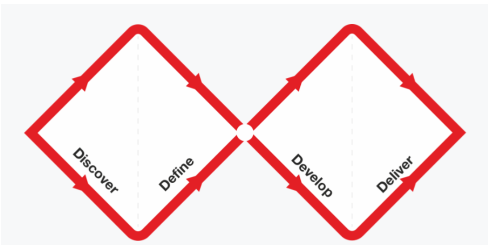

Figure 2.1: Double Diamond design process[4].

2.2 Discover

As part of the Discover phase a literature study was conducted. This process gave insight and understanding about the injection compression process as a whole, but also enabled a deeper understanding of the extrusion process and it's different components.

The literature study was done by using scientific databases such as Science Direct and Google Scholar, as well as relevant material provided from Lund University and Tetra Pak. Keywords such as *injection molding, screw design, extrusion geometry* and *polymer processing* were used to identify relevant sources. Both academic articles and industrial publications were included to ensure a balance between theoretical understanding and practical applications.

The study focused on identifying the most important geometrical parameters of the extrusion screw, such as screw diameter, pitch, channel depth and compression ratio, and how these influence the material flow and energy consumption.

The insights gained from the literature study formed the basis for selecting relevant design parameters to investigate further in the project, and guided the development of the geometric model that were developed later in the project.

2.3 Define

The Define phase focuses on narrowing down the problem and establishing the specific scope for the analysis. Based on the insights obtained in the Discover phase, the relevant geometrical input parameters and output parameters for the study were selected. The chosen input parameters were those expected to have a significant influence on the process performance, both from a theoretical and a practical perspective.

In addition to parameter selection, this phase also includes defining the constraints and parameter intervals that bound the design space. These constraints are based on a combination of existing screw geometry, machine limitations and manufacturability considerations. By defining realistic intervals, the study ensures that the evaluated designs remain feasible within the industrial context.

The Define phase therefore translates the general understanding from the Discover phase into a structured problem formulation. This provides a clear basis for the subsequent modelling and analysis in the Develop phase.

2.4 Develop

The Develop phase focuses on building and implementing the methods required to evaluate the selected parameters within the defined design space. This phase includes the development of analytical models, CAD parameterization, and the setup of the design of experiments (DOE) as well as the response surface models.

An initial attempt was made to use numerical simulation to analyse the process. However, due to limitations related to model stability and complexity, the simulation approach was discontinued. Instead, the study proceeded using analytical modelling as the main method for evaluating the process behaviour. The analytical models were implemented to describe the relationship between geometrical parameters and the output parameters, mass flow rate and power consumption.

To enable systematic variation of the geometrical parameters, a parameterized CAD model of the screw was developed. This ensured that all parameter combinations within the defined intervals could be consistently represented and evaluated.

A DOE was then constructed using response surface methodology in Minitab. The design points generated from the DOE were used together with the analytical models to calculate the corresponding output values. This enabled the construction of response surface models, which describe how the output parameters vary within the design space.

The Develop phase therefore generates the data and models required to analyse parameter trends, parameter influence and trade offs, forming the basis for the final results in the Deliver phase.

2.5 Deliver

The Deliver phase focuses on analysing and presenting the results obtained from the Develop phase. The purpose of this phase is to transform the analytical findings into practical knowledge that can be used to support extrusion screw design.

In this study, the Deliver phase includes the evaluation of the response surface models, analysis of parameter trends and parameter influence, as well as the results from the response surface optimization. These analyses provide insight into how the geometrical parameters affect mass flow rate and power consumption, and how different design objectives influence the resulting screw geometry.

3 Discover

The purpose of the Discover phase of this project is to gain as much knowledge as possible regarding the injection molding process, plastic material and the extrusion process itself. Mass flow rate and power consumption in the extrusion process will be studied in detail as well as different geometrical parameters of the extrusion screw. Research about the simulation program STAR-CCM+ and how to make a Design of Experiments in Minitab was conducted.

3.1 Injection Compression Molding

The injection compression molding process is a process that combines the advantages of conventional injection molding and compression molding. The general process of injection compression molding is the same as conventional injection molding until the point when the material exits the extruder. The process starts with the material, usually plastic granulates, being fed into the hopper. From the hopper the granulates goes into the barrel, where the screw is located. The screw's purpose is to feed the material forward while melting, mixing and pressurizing the material. As the screw rotates, the material rubs and slides against the inner surface of the barrel, along the bottom of the screw channel, at the pushing edge of the flight, and against the material itself. This movement causes the material to move forward along the screw, and the heat energy generated from the friction is absorbed by the material, which cause the melting. Additional heat is added through external heaters that are located along the outside of the barrel, to further improve the melting of the material [5]. When the material is melted the next step is to inject the material into the mold, which is where the conventional injection molding process and the injection compression molding process differ. For the injection compression molding process, which is studied in this thesis, the polymer melt corresponding to the entire volume of the molded part is inserted to a slightly opened mold. Because of the gap between the mold halves the injection pressure can be lower compared to the injection pressure for conventional injection molding, a lower injection pressure leads to a reduction of shear velocity and shear stress of the polymer melt. When the injection is done, the mold is closed by a compression step. This step is split into two sub-steps, the first is a velocity-controlled motion and when the desired clamp force is achieved the next sub-step is a force-controlled holding of the final press over the defined cooling time. By using compression molding in the last step the pressure distribution is more homogeneous, compared to using a packing method that is used in conventional injection molding. A homogeneous pressure distribution reduces the anisotropy of shrinkage, which finally results in molded parts with lower warpage, and therefore a higher dimensional accuracy. As an additional advantage, injection compression molding enables the manufacturing of thinner plastic parts [6].

3.2 Extruder

The extruder consists of the extrusion screw and the barrel surrounding the screw, see Figure 3.1. The extrusion screw runs continuously for melting and mixing the plastic granulates that enters from the hopper, and the screw is driven by an electrical motor and gearbox. The speed of the screw is set according to the plastic consumption, thus the position of the plastic accumulator is determining the speed of the extrusion screw. If the accumulator is almost empty, the screw is rotating at maximum speed, and vice versa, if the accumulator is full the screw is rotating at minimum speed [7].

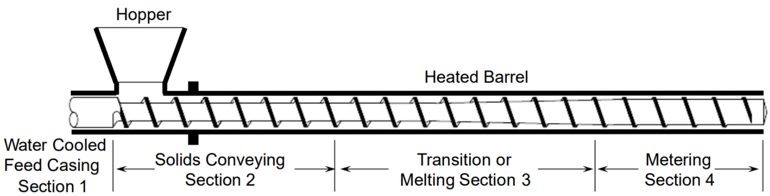

Figure 3.1: The extruder consisting of the screw and barrel[8].

The injection screw has three heating zones each consisting of two heating elements and a temperature sensor between them[7]. The first zone is the feed section where plastic enters. Here the plastic is compacted, begins to melt and is conveyed down the barrel to the next zone, which is the transition zone. In the transition zone most of the compression and melting occurs as the root diameter of the screw gradually increases, and therefore the channel depth decreases. Final melting occurs in the third zone, the metering zone. Here, the plastic melt is conveyed forward along a constant depth while reaching the necessary temperature and viscosity to form the plastic parts [9].

3.2.1 Screw

The conventional extrusion screw, and the one used at Tetra Pak, is a single flighted extrusion screw. This screw has a single helix wound around the core of the screw, shown below in Figure 3.2. Multiple flight extrusion screws on the other hand have two or more helixes started on the core, and these types of screws are high performance and common on larger-diameter extruder screws. The screw is rotated by the shank using either specially designed splines or by keys with rectangular cross sections. The zero position of the screw is set where the screw helix starts, the so called pocket. When viewing the screw from the shank looking at the tip the screw is most often rotated in a counterclockwise direction [8].

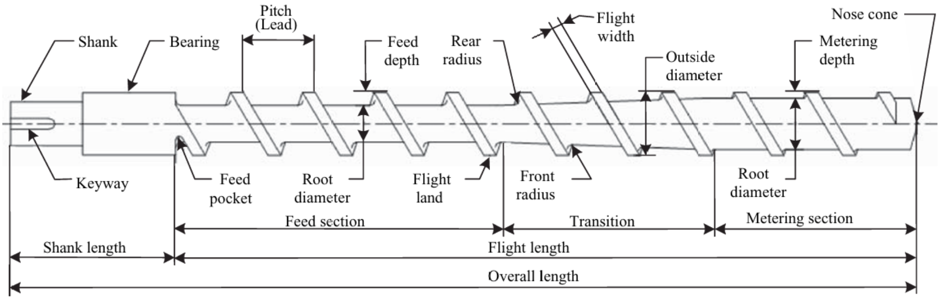

Figure 3.2: Schematic illustration of geometrical parameters on a single flighted screw [10].

3.2.1.1 L/D-ratio

The L/D-ratio is the ratio between the flighted length of the screw and the outside diameter of the screw. Most extrusion screws have a L/D-ratio in a range between 24:1 to 30:1. Extrusion screws are usually longer than injection screws, this is because in extrusion it is critical to overcome head pressure which is easier to accomplish with a longer screw. Output rates and mixing are generally also critical factors in extrusion, both of these are also easier to accomplish with a longer screw. The plastic material that is to be used also must be taken into consideration when deciding on an appropriate value for the L/D-ratio. For example, some materials that are extremely heat sensitive dictate a shorter L/D-ratio [9].

3.2.1.2 Screw Profile

The screw profile is defined as length of each of the three zones, where the length is expressed in terms of either diameter or flights. For example, a 10-5-5 screw with 20:1 L/D has 10 diameters of flighted surface in the feed zone, 5 diameters in the transition zone and 5 diameters in the metering zone [9]. General purpose screws, often have a 10-5-5 screw profile. The length of each zone has a significant impact on how the resin reaches melt condition. In a conventional extrusion screw the purpose of the feed zone is to transport the plastic pellets into the transition zone where the main purpose is to compress and melt the resin, it is in this zone that most of the pressure build-up occurs, which can be seen in Figure 3.3, which shows how the pressure in a conventional extruder rises along the screw length depending on the screws rotational speed [11]. In the metering section the main purpose is to mix and homogenize the melt [8].

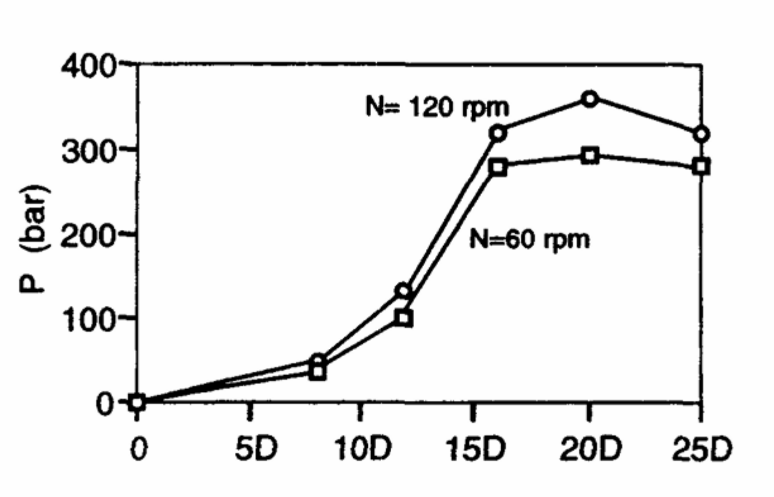

Figure 3.3: Conventional extruder pressure distribution over the length of the screw expressed in amount of diameters [11].

3.2.1.3 Flight

The flight is machined into the structure and has a helical structure that extends from the screw core to the flight tip, see Figure 3.2. At the flight tip, the flight has a certain width called flight width, and the small clearance between the flight width and the barrel wall allows the polymer to flow back towards the feed section. The polymer that does flow towards the feed section however provides support for the screw and centers it inside the barrel. The radial distance between the flight tip and the screw root is called flight height, and the channel depth is referred to as the radial distance of the flight height and the clearance together[8].

3.2.1.4 Compression Ratio

The feed zone usually has a constant core diameter with the smallest value, and the largest channel depth, and this is beneficial for conveying the plastic pellets forward to the transitions zone. In the transition zone the core diameter increases in the downstream direction, so therefore the channel depth decreases. The core diameter for the metering zone is generally constant, and the channel depth is smaller than the feed section. The ratio of the channel depth in the feed section to the channel depth in the metering section is often referred to as the compression ratio of the screw[8].

The melting performance of the screw as well as the removal of entrained air is affected by the amount and the rate of the channel depth change. During the transition section, a solid bed is formed, that is highly compressed plastic pellets that are not yet, but on its way to be molten. As compression occurs, the pellets become more compact and the voids between them disappear, thus the bulk density increases as the air is removed. Eventually, the packed pellets reaches the same density as the polymer itself, forming a fully compacted solid bed that enables stable melting and gas removal. The compression ratio, C, is calculated as followed [8].

$$C = \frac{H_f}{H} \tag{3.1}$$

Where H_f is the channel depth of the feed section, H is the channel depth of the metering section. [8]. The compression ratio typically ranges from 1.5:1 to 4:1 for most thermoplastic materials[9]. If the compression ratio is too low, the pressure build-up can be limited. An insufficient pressure build-up can limit the melting rate. If the compression ratio is too low, the feed section may not be deep enough to maintain the metering section full of resin. If the compression ratio on the other hand is too high, the pressure at the end of the transition zone may be too high causing local degradation of thermally sensitive resins. Even the flight can be severely damaged mechanically due to a too high compression ratio[8].

3.2.1.5 Pitch and Helix Angle

The pitch is the axial distance that is between one flights full turn around the screw root, see Figure 3.2. Another geometrical parameter, directly connected to the pitch is the helix angle, the correlation between these can be seen in Equation (3.2). The helix angle is the angle between a screw flight and a plane perpendicular to the screw axis. The helix angle at the barrel wall is smaller than the helix angle (at screw core) since the diameter of the barrel is considered instead of the screw core diameter[8]. On a conventionally flighted square-pitch screw, where the pitch has the same length as the screws diameter, the helix angle is approximately 17,7 degrees. Depending on the desired output, this angle can be altered. The greater the helix angle of the screw, the less shear there will be on the material. This is because there will be less flights over the length of the screw. A larger helix angle also has a larger potential mass flow rate, since there's a larger channel volume of the screw. The other way around, a smaller helix angle enables more shear on the material, and smaller potential output rates [9].

$$\theta = tan^{-1}(\frac{pitch}{\pi D}) \tag{3.2}$$

3.2.2 Barrel

In the injection compression unit the screw is inserted into the barrel. The barrel, as well as the screw, serves as an important component when transporting, melting and mixing the material. The choice of barrel directly impacts the melt quality, production efficiency and product consistency. If the selection of barrel isn't optimized for the material and product that is to be produced, this may result in material degradation, increased product defect rates or high costs for equipment maintenance [12]. When choosing the design for the barrel it is important to also have the screw in mind, since these two parts need to work together to obtain the desired output. The barrel provides a controlled environment for the plasticization process, ensuring consistent material temperature through heated zones. This ensures consistent melting of the material as it is conveyed by the screw [13]. The inside of the barrel can be designed in different ways, they are usually divided into two categories where the first one is a smooth barrel extruder, and the second one is referred to as a grooved barrel extruder. In the smooth barrel extruder, as the name implies, the entire inside of the barrel is smooth. The second category, that is used by Tetra Pak, usually has relatively deep grooves cut into the part of the barrel where the material is fed into the extruder, so called feed casing. The grooves are usually deep near the feed opening and become shallower in the downstream direction until the barrel transitions to being completely smooth. The length of the groove is typically between 3 and 5 diameters in length, whereas 3,5 is the most common. The grooves can either be positioned in the axial direction or they can be designed in a helical pattern. The grooves keep the solid GM from rotating with the screw and force the solids downstream. This mechanism can generate high pressure and dissipating a high level of energy in the grooved section. To prevent melting in the grooves, cooling of the feed casing is very important. If melting does occur the grooves can become ineffective and the solid GM's conveying can be compromised [8].

3.3 Mass Flow in Metering Section

The mass flow of the process can be approximated from calculations. The approximation of the mass flow in the metering section can act as a measure in seeing the effect from different geometrical parameters, rather than providing an exact value of the mass flow, even though the flow rate has to be within reasonable limits. To simplify the calculations and obtain a first-order engineering approximation an isothermal model is employed. This implies that the temperature of the melt is assumed to be constant throughout the studied section, and thermal effects such as heat transfer to the barrel are neglected. The model is also based on Newtonian assumptions, meaning that the viscosity of the melt is constant. Although the non-Newtonian effects has been approximated thorough a term f_L in the equation, which will be explained later in the report. The mass flow, G, is calculated from the density of the melt, ρ_m, multiplied with the volumetric flow Q, as in Equation (3.3) [10].

$$G = \rho_m \cdot Q \tag{3.3}$$

The total volumetric flow is calculated from the drag volumetric flow and the volumetric flow caused by the pressure difference. Between the flight width on the screw and the barrel there is a distance called clearance. As the pressure builds along the process, some material travels back in this space. Thus going in the opposite direction compared to the most part of the melt. This flow also has to be taken into account when calculating the total volumetric flow of the process. The volumetric flow in the metering section can be described with equation (3.4). V_{bz} is the velocity in the down channel direction, which depends on the frequency of rotation, N, diameter of the barrel, D_b and the helix angle at the barrel wall, θ_b, according to Equation (3.5). The channel width is described with W, the channel depth is described with H, and the clearance is described with δ_f, see Figure 3.4 [10].

$$Q = \frac{V_{bz}W(H-\delta_f)}{2}F_d - \frac{WH^3}{12\mu}(\frac{\delta P}{\delta z})F_p(1+f_L) \tag{3.4}$$

$$V_{bz} = \pi N D_b cos\theta_b \tag{3.5}$$

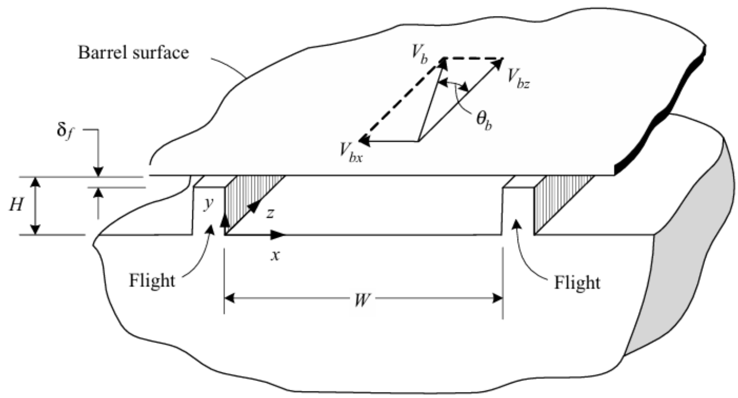

Figure 3.4: Velocity vectors in the screw channel [10].

In the equation describing the total volumetric flow, Equation (3.4), F_d and F_p are "shape factors" for the drag and pressure flow. They assume values that are smaller than one and represent the restricting effect of the flight on flow between parallel plates, it is a function of the H/W ratio. The mathematical description for the factors is seen in (3.6) and (3.7). The factors are plotted in Figure 3.5 [10].

$$F_d = \frac{16W}{\pi^3 H} \sum_{i=1,3,5}^{\infty} \frac{1}{i^3} \tanh\left(\frac{i\pi H}{2W}\right) \tag{3.6}$$

$$F_p = 1 - \frac{192H}{\pi^5 W} \sum_{i=1,3,5}^{\infty} \frac{1}{i^5} \tanh\left(\frac{i\pi W}{H}\right) \tag{3.7}$$

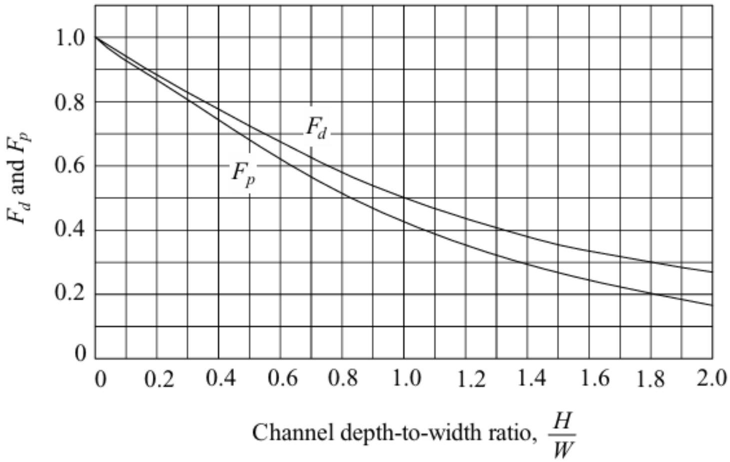

Figure 3.5: Shape factors, F_d and F_p [10].

In Equation (3.4) the term with delta pressure divided with delta helical length, $\frac{\delta P}{\delta z}$, represents the pressure difference over the metering section, with the axial length, L_m, see Equation (3.8). The f_L term is an approximation of the non-Newtonian effects. It attempts to evaluate the viscosity, μ, at the prevailing shear rates in the clearance. The f_L term is given from Equation (3.9). Where the flight width is described with e, and the melt viscosity by the screw core is described with μ and the viscosity by the flight is described with μ_f [10].

$$\frac{\delta P}{\delta z} = \frac{\delta P \cdot sin\theta_b}{L_m} \tag{3.8}$$

$$f_L = (\frac{\delta_f}{H})^3 \frac{e}{W} \frac{\mu}{\mu_f} + \frac{(1+\frac{e}{W})[\frac{1+e/W}{tan^2\theta} + \frac{6\mu V_{bz}(H-\delta_f)}{H^3(\partial P/\partial z)}]}{1+\frac{\mu}{\mu_f}(\frac{H}{\delta_f})^3 \frac{e}{W}} \tag{3.9}$$

3.3.1 Viscosity

The viscosity of a polymer depends on several parameters such as its phase as well as pressure, temperature and shear rate. The Cross-WLF viscosity model is a rheological model for describing non-Newtonian polymer melts [14]. It describes how the temperature, shear rate and viscosity are correlated, and the melt viscosity, is given by Equation (3.10) where $\dot{\gamma}$ is the shear rate. The zero shear viscosity, μ_0, is where the viscosity approaches a constant at very low shear rates. The critical stress level at the transition to shear thinning, τ^*, and the power law index in the high shear rate regime, n, is determined by curve fitting.

$$\mu = \frac{\mu_0}{1 + (\frac{\mu_0 \cdot \dot{\gamma}}{\tau^*})^{1-n}} \tag{3.10}$$

The zero shear viscosity is presented in Equation (3.11) below, where D_1 and A_1 are data-fitted coefficients, depending on the studied material. The temperature, T, is in Kelvin and T^* is the glass transition temperature and this parameter is determined by curve fitting. The parameter A_2 varies with pressure and data-fitted coefficients.

$$\mu_0 = D_1 \cdot EXP(-\frac{A_1(T - T^*)}{A_2 + (T - T^*)}) \tag{3.11}$$

The glass transition temperature is given by Equation (3.12) where D_2 and D_3 are data-fitted coefficients and p is the pressure.

$$T^* = D_2 + D_3 \cdot p \tag{3.12}$$

The equation for A_2 is given by Equation (3.13) where $\tilde{A}_2$ is a data-fitted coefficient.

$$A_2 = \tilde{A}_2 + D_3 \cdot p \tag{3.13}$$

The average shear rate used in Equation (3.10) represents the mean shear rate experienced by the material and is used as a simplified measure in the isothermal model. The average shear rate depends on the diameter of the screw, D_s, frequency of rotation and the channel depth, as seen in Equation (3.14).

$$\dot{\gamma} = \frac{\pi D_s N}{H} \tag{3.14}$$

The shear rate differs depending on where in the screw the material is located. It depends on what section of the screw the material is in, since the screw diameter changes from the different sections. It also depends on where in the section the material is located. The material located in the clearance between the flight width and barrel is exposed the a higher shearing, since the diameter of the screw then also includes the flight.

3.4 Energy Consumption

The total shaft power input, P_w, is calculated according to Equation (3.15) where a negligible leakage over the screw flights is assumed. Where L is the total length and $\overline{\theta}$ is the average helix angle at screw core, and the ratio between them expresses the helical channel length. The ratio, $\frac{Q}{Q_d}$, varies depending on if the discharge is closed or open. Closed discharge occurs when the net flow through the outlet is zero, $Q = 0$. Thus, the pressure-driven flow balances the drag flow in the opposite direction, so the screw operates against a fully restricted outlet, leading to a maximum pressure build-up and therefore maximum mechanical load. Open discharge on the other hand, corresponds to an unrestircted outlet condition, with no pressure build-up in the channel. The net flow equals to drag-induced flow, $Q = Q_d$, resulting in the maximum volumetric flow rate and a lower mechanical load on the screw. For open discharge, the ratio, $\frac{Q}{Q_d}$ equals 1 while it equals 0 for a closed discharge [10].

$$P_w = \mu \cdot \frac{\pi^2 N^2 D_b^2 W L}{sin\overline{\theta} H}(4 - 3cos^2\theta_b \frac{Q}{Q_d}) \tag{3.15}$$

3.5 Plastic Material

The injection compression molding of the top is conducted directly onto the paperboard. The material for the top is HDPE which is a semi-crystalline polymer, and is a suitable material for injection compression molding due to its properties such as high strength to weight ratio, high impact resistance, durability and movability [15].

In the extruder, polymer degradation may occur unless precautions are taken to minimize the reactions. Polymer degradation refers to polymers losing their original properties as a result of the surrounding environment. Heat, light, water, and air are some factors that affect polymer degradation, leading to chemical changes. In the extruder, a common reason for degradation is to high shear stress related to high polymer viscosity, leading to the loss of a hydrogen atom. This radical reacts with oxygen from the atmosphere and causes chemical reactions. In order to minimize polymer degradation during extrusion processes, stabilizers and additives can be added to the polymer [8]. Also, designing a screw that provides the right amount of shearing will decrease the risks of degradation.

The melting temperature is the peak temperature where most of the crystals are melted. The glass transition temperature is the temperature where the hard and brittle, ”glassy” polymer translates to a softer and flexible, ”rubbery” state. So, the glass transition temperature influences the material’s performance in different thermal environments while the melting temperature determines the processing conditions [8].

3.6 STAR-CCM+

The computer program used for the simulations in this thesis project was STAR-CCM+ which primarily is a computational fluid dynamics (CFD) solver developed by Siemens Digital Industries Software. STAR-CCM+ focuses on fluids, heat transfer and flow-related multiphysics. Before executing a STAR-CCM+ simulation, a series of pre-processing steps must be completed to ensure that the model accurately represents the physical system. These steps are presented in more detail below [16].

3.6.1 Geometry preparation

The initial step to perform a simulation in STAR-CCM+ is to import the 3D model used into the interface of STAR-CCM+. The 3D model of the extrusion screw will be modelled and modified in Creo Parametric. Creo Parametric is a leading 3D CAD software developed by PTC and provides the tools necessary for modern product design and development [17].

3.6.2 Physics Models

Selecting an appropriate physics model is a fundamental step in setting up a simulation in STAR-CCM+, as it determines which physical phenomena are solved and how the governing equations are formulated. The choice of physics models depends on factors such as flow regime, material behavior, thermal effects, and whether the simulation is steady-state or transient. For extrusion-related flows, this typically involves selecting a fluid flow model, defining the material properties, and enabling turbulence, heat transfer, or rotating reference frame models. An over-simplified physics model may neglect important effects, while an overly complex model can lead to unnecessary numerical difficulties and increased computational cost. As a result, the physics model should be selected to balance accuracy, stability, and feasibility within the scope of the study [18].

3.6.3 Boundary Conditions

Boundary conditions define how the computational domain interacts with its surroundings and are required to be assigned appropriate physical conditions before a simulation can be run. Typical boundary conditions are an inlet, an outlet and solid walls. At the inlet, either a velocity inlet or mass flow inlet can be used depending on the known process parameters. At the outlet, a pressure outlet is commonly used, allowing the solver to determine the outlet velocity field while maintaining a specified reference pressure. No-slip walls is another boundary condition that can be used for example between the screw and barrel surfaces to correctly capture viscous effects and shear stresses. If screw rotation is considered, a rotating wall condition can be applied to the screw surface. In addition, suitable initial conditions for variables such as velocity and pressure must be specified to support numerical stability and convergence [18].

3.6.4 Mesh

Meshing is a crucial step of the simulation process in STAR-CCM+ for accurately simulating fluid flow. Meshing means breaking the geometric volume down into small elements which are connected through nodes, in which the governing equations are solved numerically [18].

For complex geometries, such as extrusion screws, mesh quality strongly influences both accuracy and numerical stability. The mesh must be fine enough to resolve narrow gaps and regions with high velocity gradients, while avoiding excessive cell counts that increase computational cost [18].

A volume mesh is a discrete representation of a continuous volume. A high quality volume mesh is essential for an accurate, stable and converged solution. Some unstructured volume mesh models in STAR-CCM+ are trimmed cell, tetrahedral and polyhedral. Polyhedral meshes are often preferred for internal flows with strong rotation or swirl, and complex industrial geometries where robustness and numerical stability are prioritized [18].

3.7 Minitab Statistical Software

Minitab Statistical Software tool is commonly used for data analysis and process improvement. In this study, it is used to perform DOE, which allows systematic variation of input parameters to analyze their influence on selected responses. The software is also used to generate response surface models and support optimization of the extrusion screw geometry [19].

3.8 Design of Experiments

A DOE, is a series of runs in which the responses are observed while the input variables change. Several types of DOE exist, each serving different purposes. Screening design, factorial design, and response surface design are some of them. A screening design is often used in the early stages of identification of the most influential factors among a large number of possible parameters. These designs primarily focus on estimating the main effects and assume linear relationships between factors and response[20]. Factorial designs usually operate at two levels per factor and are effective for understanding factor interaction, however, they have limited capability to model curvature in the response [21].

A response surface DOE is an advanced DOE technique that is used to optimize the response. The response surface methodology is often used when curvature in the response surface is suspected, and it is used to refine models after determining important factors. Response surface methodology is commonly implemented using Central Composite Designs (CCD) or Box-Behnken Designs (BBD). The CCD is composed of three types of experimental points: factorial, axial and center points. This structure allows for a fully quadratic model, a second-order regression model that includes linear terms, interaction effects and square terms. BBD can also estimate a full quadratic model, but usually with fewer design points than CCD, and therefore they require fewer experimental trials. BBD does not include runs from a factorial experiment, and BBD never include runs where all factors are at their extreme setting, such as all the low settings [22].

CCD is preferred when sequential experimentation and model flexibility are required while BBD is advantageous when the number of experimental trials and avoidance of extreme factor combinations are primary concerns. A face-centered CCD is a type of CCD in which the axial points are located at the center of each face of the factorial cube [22].

A response optimization identifies the combination of variable settings that optimize a single response or a set of responses. The Response Optimizer in the statistical software Minitab searches for optimal responses based on the requirements that are set for each response. The response can be minimized, maximized, or defined to reach a target value. When multiple responses are considered simultaneously, each response is transformed into a desirability value between 0 and 1, representing how well the response meets its objective, where 1 represents full desirability [23].

The weight parameter controls how quickly desirability decreases as the response moves away from the desired value. For target based optimization, a higher weight results in a narrower desirability peak around the target, meaning that solutions close to the target are preferred, while deviations are penalized more strongly, see Figure 3.6 [24]. The importance factor defines the relative priority of each response when trade-offs between multiple objectives are required [23].

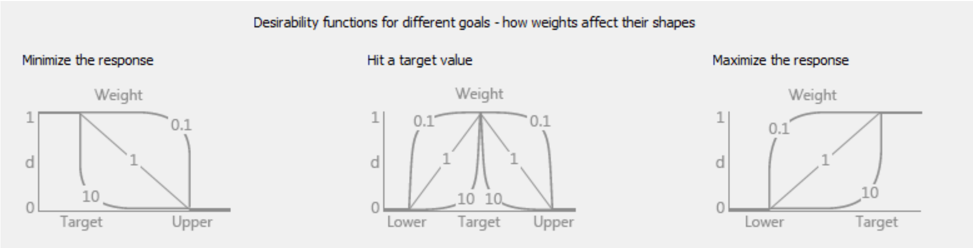

Figure 3.6: Weight factor's effect on the desirability function[24].

The individual desirability values are combined into a single metric called composite desirability, which represents the overall quality of a solution with respect to all response objectives [23]. The composite desirability is calculated automatically in Minitab according to Equation 3.16 as a weighted geometric mean of the individual desirability values. d_i is the individual desirability for the i^{th} response, w_i is the importance of the i^{th} response and W is the sum of the different w_i [25]. The solution with the highest composite desirability is identified as the optimal compromise [23].

$$D = (\Pi(d_i^{w_i}))^{\frac{1}{W}} \tag{3.16}$$

4 Define

Based on the findings during the Discover phase, conclusions and assumptions about the selected input parameters as well as the output parameters were defined. During the Define phase, constraints and parameter intervals were also defined.

4.1 Selected Geometrical Parameters

The geometrical parameters selected for furthered study where chosen based on considerations from both the analytical and the numerical modeling approaches explored during the Discover phase.

From an analytical modeling perspective, the selected parameters were those that, according to the analytical model, were expected to have a direct influence on the mass flow rate and the energy consumption of the process.

For the numerical modeling approach, some practical considerations were taken into account. Since STAR-CCM+ relied on a parametric CAD model, the geometrical parameters needed to be suitable for an efficient parameterization and modification of the model. The selected parameters were thus those that were most intuitive and feasible to define as driving dimensions in the CAD model.

The final geometrical input parameters were selected as a compromise between analytical relevance and practical suitability for parametric CAD-driven numerical modeling. The selected parameters were clearance, diameter screw core metering, axial channel width metering, axial flight width metering and flight height metering, see Figure 4.1 below. The axial flight width, e_{axial}, is the length of the flight width in the axial screw direction, and the axial channel width, W_{axial}, is the length of the channel width in the axial screw direction. They were chosen as input parameters since those are the driving parameters in the CAD model, which from Equation (4.1) and Equation (4.2) gives the flight width and channel width used for the mass flow rate and power consumption [10].

$$e = e_{axial} \cdot cos\theta \tag{4.1}$$

$$W = (W_{axial} + e_{axial}) \cdot cos\theta - e \tag{4.2}$$

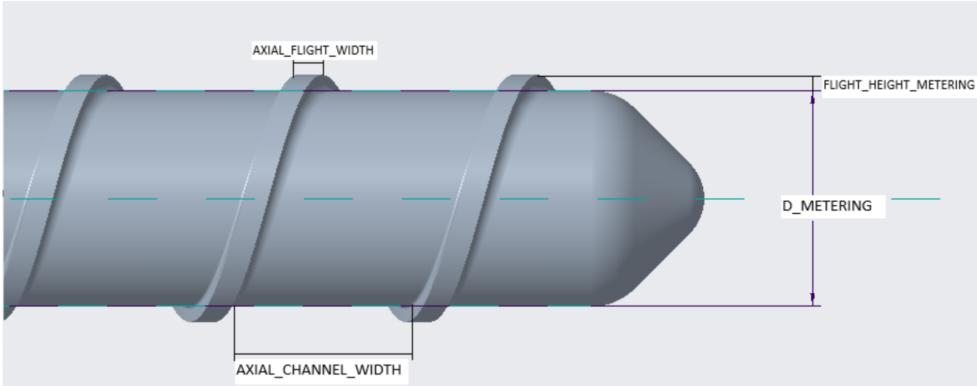

Figure 4.1: Chosen input parameters illustrated in CAD model.

4.2 Selected Output Parameters

The selected output parameters for evaluating extrusion screw performance were mass flow rate and power input. These parameters were chosen because they are directly linked to processing efficiency and operational cost, which aligns with the main objective to increase output while optimizing cost. The chosen output parameters was also an interest from Tetra Pak's side to know more about. Mass flow rate represents the productivity of the extrusion process, while energy consumption has a strong impact on operating cost, as higher energy usage directly results in higher production cost. Evaluating both parameters therefore enables an assessment of how changes in screw geometry affect output efficiency from both a performance and a cost-related perspective.

Other aspects, such as mixing quality and melting efficiency, are also important for extrusion performance. However, these phenomena are difficult to evaluate without experimental testing of the extruded material. Such testing was outside the scope of this thesis due to time constraints.

4.3 Constraints & Parameter Intervals

To achieve a reasonable response surface appropriate parameter intervals had to be chosen. The intervals were determined based on the dimensions of the current screw.

When setting up the parameter intervals it was made sure that all the parameters within the interval was possible to manufacture, this was made sure by testing the maximum and minimum values in the created CAD-model as well as confirmed with the engineering team at Tetra Pak. Manufacturability is not the only constraint for the parameters, the material also needs to be properly mixed and melted. But this is not evaluated in this thesis, therefore that was not considered more than that the screw looked reasonable.

The current screw has a L/D-ratio outside of the recommended values presented in Section 3.2.1.1, and therefore the length of the screw was extended to a constant value. That was because there is limited space in the machine, so for the screw to be able to fit together with the rest of the components the length was kept constant at the maximum possible length. The length of the metering section was set to the same percentage of the whole length as the current screw has, and is therefore also kept constant. The relationship was set as constant because the material needs to be melted and mixed properly, which is process parameters that is not evaluated in this thesis, therefore the current relationship is kept, and the length is not made shorter.

The interval for the clearance was based on the tolerances from the drawing of the current screw. The maximum value was the largest achievable gap that is possible with the current tolerances. The minimum value was set 30% below the current value. The parameters flight height, h_f, axial channel width, w, and axial flight width, e_{axial}, had the minimum and maximum value of $\pm$30 % of the current parameter value. The interval $\pm$30% was chosen since that was seen as broad enough to give an overview of the sensibility for the parameter while still having minimum and maximum values that was possible to manufacture.

The interval for the screw root diameter in the metering section, D_s, was set up with the limits for the L/D-ratio in mind. From the discover phase it was stated that the L/D-ratio for an extrusion screw should be between the ratios 24:1 and 30:1. Therefore the interval for the diameter of the screw core had these ratios as guidance, but the L/D-ratio is based on the outer diameter of the screw, i.e. the screw core diameter plus two flight heights. So the minimal and maximum core diameter of the screw was calculated according to Equations (4.3) to (4.6).

$$\frac{L}{D_{min}} = 30 \implies D_{min} = \frac{L}{30} \tag{4.3}$$

$$\frac{L}{D_{max}} = 24 \implies D_{max} = \frac{L}{24} \tag{4.4}$$

$$D_{min} = D_{s,min} + 2h_{f,min} \implies D_{s,min} = D_{min} - 2h_{f,min} = \frac{L}{30} - 2h_{f,min} \tag{4.5}$$

$$D_{max} = D_{s,max} + 2h_{f,max} \implies D_{s,max} = D_{max} - 2h_{f,max} = \frac{L}{24} - 2h_{f,max} \tag{4.6}$$

5 Develop

The Develop phase of this project included developing the simulation model and the analytical calculations as well as their validation through physical testing. During this stage, the CAD model was also created and parameterized. Additionally, the Design of Experiments and response surface optimization were developed.

5.1 Numerical Simulation

The initial objective of the simulation work was to utilize a fully operational CFD model in STAR-CCM+ provided by the project stakeholders, which would enable numerical investigation of the flow and process behavior. However, the simulation model that was made available was incomplete and required additional setup before it could be used for reliable analysis.

Completing the model involved defining regions, interfaces, and boundary conditions, as well as verifying mesh settings and solver settings. This process demanded advanced CFD expertise and extensive knowledge of STAR-CCM+ which was beyond the scope of the project. Despite iterative attempts to troubleshoot the model through testing different boundary conditions, region definitions, and solver settings, stable and reliable simulation results could not be achieved within the project timeframe.

Given these limitations, and in order to ensure progress and maintain technical reliability, the decision was made to discontinue further CFD development. Instead, the study proceeded using analytical calculations based on the established theoretical models and assumptions. This approach provided sufficient accuracy for the purpose of the project while remaining feasible within the available time and level of expertise.

5.2 Analytical Calculations

From the Discover phase, models regarding the mass- and volumetric flow was found. Different sources provided different equations, where a lot of simplification had been made. Therefore it was necessary to make sure that the simplifications were appropriate for Tetra Pak's process. The chosen equation for the volumetric flow, Equation (3.4), is an isothermal Newtonian model, but it approximates the non-Newtonian aspects through the leakage flow correction factor, f_L, which was seen necessary since there can be a significant difference for the viscosity of the polymer in the clearance compared to the viscosity by the screw root. The model is also based on isothermal conditions, which in reality a viscous flow never truly can be. But to make a first order approximation of the flow, it was a necessary simplification to make, since the difference between the geometric parameters still would be valid. In order to make sure that the model for the volumetric flow was accurate for Tetra Pak's process, comparison with previously conducted physical tests on the extruder was done.

5.2.1 Verification of Mass Flow Rate with Physical Tests

To verify that the equations from the literature study was accurate and could be used for Tetra Pak's process the equation for the volumetric flow in the metering section was calculated with the dimensions and values for the current extruder, and the results from the calculations was compared to physical tests that previously had been performed by the company. All calculations was performed in Microsoft Excel.

The dimensions for the geometrical parameters was obtained from the drawings of the screw that is used in the machines in the test hall at Tetra Pak. The helix angle at the barrel wall, θ_b, was calculated by using Equation (3.2), where the pitch is the sum of the axial channel width and axial flight width, see Equation (5.1).

$$\theta_b = tan^{-1}(\frac{pitch}{\pi D_b}) = tan^{-1}(\frac{W_{axial} + e_{axial}}{\pi D_b}) \tag{5.1}$$

The shape factors F_d and F_p were calculated using the analytical expression given in Equations (3.6) and (3.7), rather than being estimated from the graphical representation shown in Figure 5.1.

Both equations contain an infinite series over odd values of the index i. To evaluate these series numerically, the individual terms were calculated separately in Excel for successive odd values of i (i = 1,3,5,...). For each value of i, the corresponding term of the series was computed and added to a cumulative sum.

The series was truncated at $i = 53$, as contributions from higher-order terms were found to be negligible compared to the total value. The individual contributions of each term, as well as the resulting cumulative sums for F_d and F_p, are presented in Table 5.1. After evaluating the series, the obtained sums were multiplied by the remaining prefactors in Equations (3.6) and (3.7) to determine the final values of the shape factors F_d and F_p.

Table 5.1: Individual contributions and cumulative sum of the series used to evaluate the shape factors F_d and F_p.

i	F_d	F_p
1	0.126004	1
3	0.013435	0.004115226
5	0.004483	0.00032
7	0.002069	5.9499×10^{-5}
9	0.001117	1.69351×10^{-5}
11	0.000664	6.20921×10^{-6}
13	0.000423	2.69329×10^{-6}
15	0.000283	1.31687×10^{-6}
17	0.000198	7.04296×10^{-7}
19	0.000143	4.03861×10^{-7}
21	0.000107	2.44852×10^{-7}
23	8.17×10^{-5}	1.55368×10^{-7}
25	6.38×10^{-5}	1.024×10^{-7}
27	5.07×10^{-5}	6.96917×10^{-8}
29	4.09×10^{-5}	4.8754×10^{-8}
31	3.35×10^{-5}	3.49294×10^{-8}
33	2.78×10^{-5}	2.55523×10^{-8}
35	2.33×10^{-5}	1.90397×10^{-8}
37	1.97×10^{-5}	1.44209×10^{-8}
39	1.69×10^{-5}	1.10835×10^{-8}
41	1.45×10^{-5}	8.63139×10^{-9}
43	1.26×10^{-5}	6.80233×10^{-9}
45	1.10×10^{-5}	5.41923×10^{-9}
47	9.63×10^{-6}	4.36024×10^{-9}
49	8.50×10^{-6}	3.54013×10^{-9}
51	7.54×10^{-6}	2.89834×10^{-9}
53	6.72×10^{-6}	2.39123×10^{-9}
Sum	**0.149355**	**1.004523748**

The viscosity in the channel as well as the flight was calculated using the Cross-WLF viscosity model, see Equation (3.10). First the zero shear viscosity, Equation (3.11), was calculated. All the material and process parameters was provided by the company. Then the average shear rates for the current process was calculated from Equation (3.14), both in the channel and by the flight. To calculate the average shear rate in the channel the measurements for the diameter by the screw core and channel depth was used. To calculate the average shear rate by the flight the flight height was multiplied with two and then added to the screw core diameter, which gave the diameter of the screw including the flights. Since there is no channel depth by the flights, the clearance was used instead, which by the flights is the radial distance to the barrel wall. The expression can be seen in Equation (5.2).

$$\dot{\gamma_f} = \frac{\pi(D_s + 2h_f)N}{\delta_f} \tag{5.2}$$

In the expression for the volumetric flow the term regarding the pressure build-up over the metering sections helical length had to be approximated, since there was no data regarding this from previous tests that the company had conducted. To make an approximation about this it was assumed that the pressure build-up in the metering section corresponded to 10% of the total pressure rise in the process. The percentage was assumed since it was stated from the discover phase that the most part of the rise in pressure is generated in the transition section and not in the metering section. So to assume a 10% pressure rise in the metering section was considered a conservative assumption since in reality it would probably be smaller. To achieve a more exact value for this term in the future, simulations or physical testing with pressure sensors is recommended.

To calculate the f_L term Equation (3.9) was used. Where the geometric parameters from the drawing was inserted, as well as the approximated value for the pressure build-up over the metering section and the calculated viscosities. The helix angle for the screw was calculated using Equation (3.2), and the axial velocity V_{bz} was calculated using Equation (3.5).

From these calculations the volumetric flow could be calculated, using Equation (3.4). Which then was multiplied with the average melt density for the processed material, provided by the company. The theoretical approximation of the mass flow could then be verified with the physical test results, to make sure that the formulas was accurate for Tetra Pak's process. When comparing the results it was shown that the result from the calculations was in line with the result from the physical test. To make sure that the model was accurate, the mass flow at different rotational screw speeds was plotted and compared to the results from the physical tests at the same screw speed. The result shows a similar shape for both curves, but the calculated mass flow curve is slightly flatter than the experimentally measured values, see Figure 5.1 and 5.2. In Figure 5.1 the different lines represent different accumulator pressures, and the pressure compared with and used in the analytical calculation was a pressure in between the red and green line. This verified that the method for calculating the mass flow could be used, since the shapes of the lines were rather close to each other.

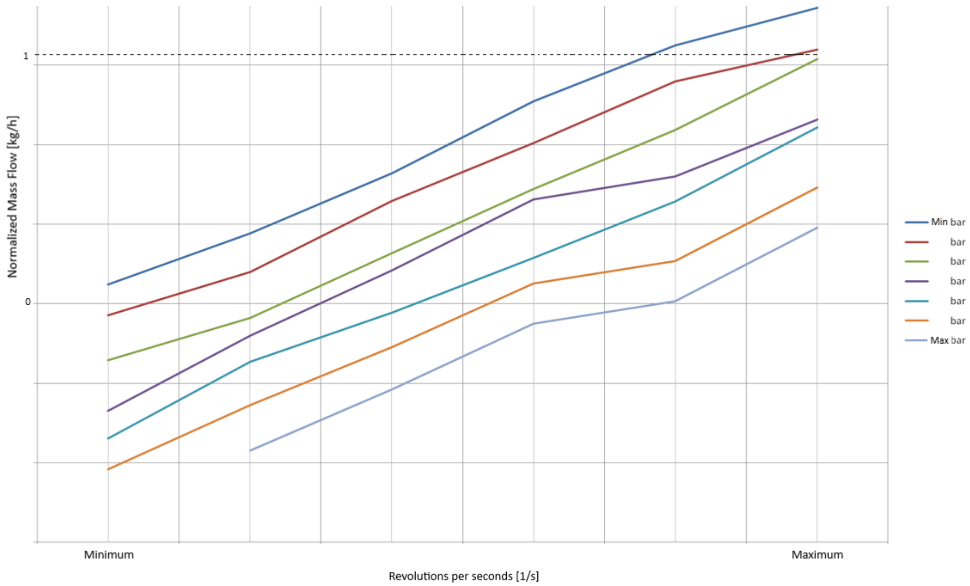

Figure 5.1: Normalized mass flow rate curve at different screw speeds and pressures, measured from physical experiments. The pressure used for the calculation is between the green and red line.

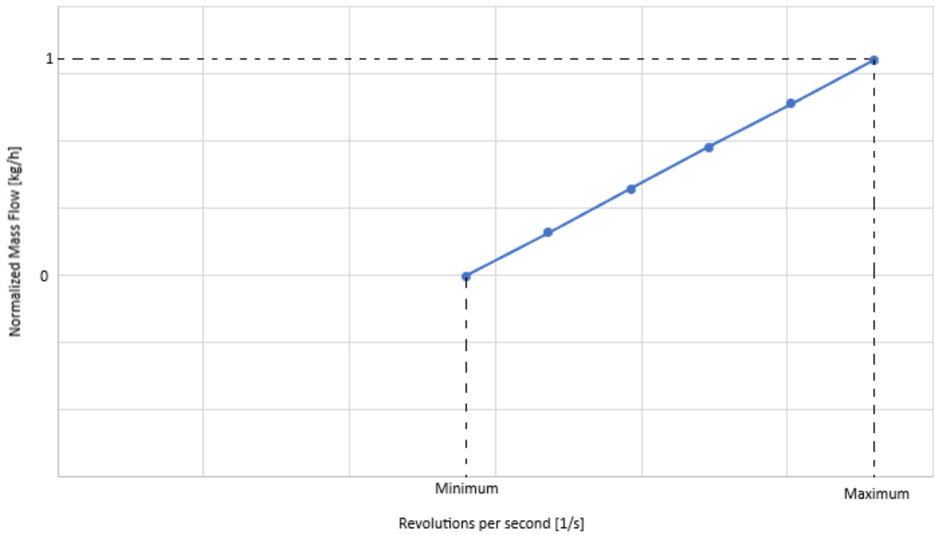

Figure 5.2: Normalized mass flow rate curve at different screw speeds, achieved from analytical calculations.

5.2.2 Verification of Power Consumption with Physical Tests

The formula for the total shaft power input was calculated and compared to previously performed tests. The average helix angle at screw core, $\overline{\theta}$, was determined by calculating the value of the helix angle at screw core in the feed section as well as in the metering section with Equation (5.3) and (5.4) that are modifications from Equation (3.2). The core diameter in the feed section was restricted to be 6 mm smaller than the core diameter in the metering section for a smooth transition between all three sections.

$$\theta_{s,feed} = tan^{-1}(\frac{pitch}{\pi D_{s,feed}}) = tan^{-1}(\frac{W_{axial} + e_{axial}}{\pi D_{s,feed}}) \tag{5.3}$$

$$\theta_{s,metering} = tan^{-1}(\frac{pitch}{\pi D_{s,metering}}) = tan^{-1}(\frac{W_{axial} + e_{axial}}{\pi D_{s,metering}}) \tag{5.4}$$

From this, the average helix angle at screw core, $\overline{\theta}$, was calculated according to Equation (5.5).

$$\overline{\theta} = \frac{\theta_{s,feed} + \theta_{s,metering}}{2} \tag{5.5}$$

The extruder in the present system operates against a downstream accumulator, which imposes a back pressure on the polymer melt and prevents free outflow form the screw channel. Consequently, the outlet is pressure-restricted and could not be treated as an open discharge. To obtain a conservative and physically representative estimate of the required mechanical power, the process was therefore modeled under closed discharge conditions, corresponding to zero net flow ($Q = 0$) and maximum mechanical load.

From these calculations and assumptions, the total shaft power input was calculated using Equation (3.15). This theoretical power requirement was compared with experimental measurements performed at a corresponding motor frequency. At this operating point, the physical test result showed a power consumption of the motor about twice as high as the calculated required power. Consequently, the theoretical model underestimated the measured power demand. Despite this deviation, the theoretical value was considered suitable as an order-of-magnitude estimate and could serve as an useful indicator of the mechanical load on the screw rather than as an exact quantitative prediction.

5.3 CAD-modeling & Parameterizing

A three dimensional CAD model of the screw was developed and parameterized to support future numerical simulations. The original CAD model provided was modeled in a way that made geometric modifications difficult, particularly when changing key dimensions. Therefore, a new model was created based on the parameters intended to be varied, and explicit relationships were defined between these parameters to ensure consistent geometry updates. The screw was modeled using dimensions of the existing screw as a baseline. The resulting parametric model enabled systematic variation of design parameters and was used to establish and verify constraints between parameters, ensuring that the geometry remained physically reasonable and that the model regenerated successfully for all relevant parameter combinations.

The CAD model was developed with some different features in Creo Parametric. First, a revolve was created around the screw axis with a smooth transition between the feed core diameter and the metering core diameter. The key dimensions such as the core diameter of the feed section, the core diameter of the metering section as well as the lengths of the feed zone, metering zone, and the total screw length, were assigned to already defined parameters in Relations, see Figure 5.3. All parameters used in Relations are described and defined in Table 5.2. The tip of the screw was included in the revolve feature while the start of the screw, the part of the screw connected to the injection molding machine motor, was modeled by two different extrudes as shafts. The flights of the screw were modeled using a helical sweep operation. The helical sweep was defined using a helical path that was oriented parallel to the screw axis along the screw core. A cross-sectional sketch defining the flight geometry was created normal to the helical path. In the sketch, the flight profile was defined radially from the helical axis up to the specified flight height. The flight height and flight width were fully parameterized and controlled by previously defined design parameters. The pitch of the helical sweep was also defined as a parameter, allowing systematic variation of the channel geometry, and a left handed helical direction was selected. The helical sweep extended continuously along the length of the screw up to the screw tip, resulting in a single, continuous flight across the feed, transition, and metering sections, see Figure 5.4 below.

```
L_METERING = (150/732) *L_TOTAL

L_TRANSITION = L_TOTAL - L_FEED - L_METERING - 19

FLIGHT_HEIGHT_FEED = FLIGHT_HEIGHT_METERING + R_METERING - R_FEED

R_METERING = D_METERING / 2

R_FEED = R_METERING -3

PITCH = AXIAL_FLIGHT_WIDTH + AXIAL_CHANNEL_WIDTH

L_PITCH = L_TOTAL  - AXIAL_FLIGHT_WIDTH -19
```

Figure 5.3: Assigned relations in Creo Parametric.

Table 5.2: Description of screw geometry parameters.

Parameter	Description
L_TOTAL	Total screw length
L_METERING	Length of the metering zone
L_TRANSITION	Length of the transition zone
L_FEED	Length of the feed zone
L_PITCH	Effective pitch length along the screw
D_METERING	Diameter of the metering section
R_METERING	Radius of the metering section (half of D_METERING)
R_FEED	Radius in the feed zone
FLIGHT_HEIGHT_FEED	Flight height in the feed zone
FLIGHT_HEIGHT_METERING	Flight height in the metering zone
AXIAL_FLIGHT_WIDTH	Width of the flight in the axial direction
AXIAL_CHANNEL_WIDTH	Width of the channel in the axial direction
PITCH	Screw pitch (sum of axial flight width and axial channel width)

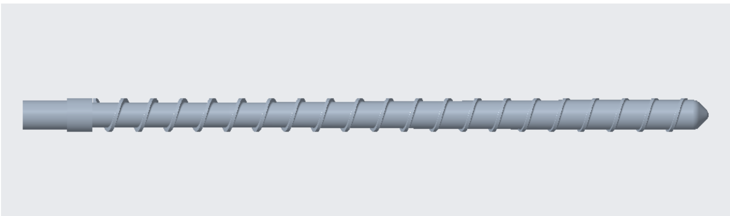

Figure 5.4: CAD model of the current extrusion screw.

5.4 Design of Experiment

When the equations for the current screw had been verified with physical tests and the CAD-model had been made, a DOE was set up in order to analyse the impact of each geometrical parameter. The DOE was made in the program Minitab.

In Minitab a Response Surface DOE was set up. Response surface was the chosen type since the selected parameters could have a non-linear influence on the response, and therefore a curvature response was desirable. Screening designs typically assume linear relationships between factors and response and they are mainly intended for the early identification of significant factors. Similarly, while factorial designs are effective for studying interaction effects, their two-level structure limits their ability to capture curvature in the response surface. A response surface DOE on the other hand, allows estimation of a full quadratic model, enabling a more accurate representation of the underlying process behavior and supporting response optimization. Consequently, a response surface DOE was considered the most suitable approach.

The number of continuous factors was set to five, since that was the amount of parameters that was to be varied. The maximum and minimum values for each parameters were also assigned based on the predefined constraints and intervals described in Section 4.3. A full, unblocked central composite design was selected because the response values were calculated using analytical models rather than obtained from physical experiments. Consequently, no time-dependent or batch-related variations were present, and all design points were evaluated under identical conditions.

A face centered design was used, corresponding to an axial distance of $\alpha = 1$, ensuring that all axial points were located within the specified factor ranges. Run randomization was not required since the study was based solely on analytical model evaluations.

Based on these settings, a total of 52 design points were generated for the response surface DOE. These points were used as input in an Excel spreadsheet to calculate the response values using the analytical mass flow model as well as energy consumption model. The resulting data were then imported into Minitab for response surface analysis.

Before executing the response surface analysis some settings had to be done. The response variables were defined as mass flow rate and power consumption. Stepwise regression was used to retain statistically significant model terms and simplify the resulting model.

5.5 Response Surface Optimization

Based on the two response surfaces obtained for mass flow rate and power consumption, several response optimization problems could be formulated using the Response Optimizer. An initial optimization was performed with the objective to maximize mass flow rate while minimizing power consumption. In this optimization, the weight and importance factors were kept unchanged, as the purpose was to explore the overall trade-off between the two responses rather than to prioritize one response over the other.

In addition to this initial optimization, three further response optimizations were set up. These optimizations were defined to ensure that the developed framework would be applicable across the full range of relevant operating conditions within the Tetra Top process, rather than focusing only on maximizing the mass flow rate, which represents only the largest top. By considering multiple optimization scenarios, the framework was developed to support design decisions for different production requirements.

First, an optimization was conducted for the largest top. In this case, power consumption was minimized, while the mass flow rate was defined with a target objective. The target value was set to the required material throughput for manufacturing the highest volume, including a safety factor of 10%. The weight factor for mass flow rate was increased to 10, while the weight factor for power consumption was kept at its default value of 1. This was done to ensure that the optimization focused on solutions close to the specified target mass flow rate. The same optimization procedure was then applied to the medium-sized top and the smallest top, corresponding to lower required material throughput levels.

6 Deliver

In the Deliver phase of the project, the findings from the numerical simulation and analytical models were compiled and presented. This included insights from parameter trends, response surface results, parameter influence, residual analysis, and response optimization.

6.1 Numerical Simulation

The residual plot indicates that the simulation model did not reach convergence. While the residuals initially decrease, they later increase again and show strong oscillations, see Figure 6.1. This indicates numerical instability and suggests that a steady and converged solution could not be obtained for the numerical simulation.

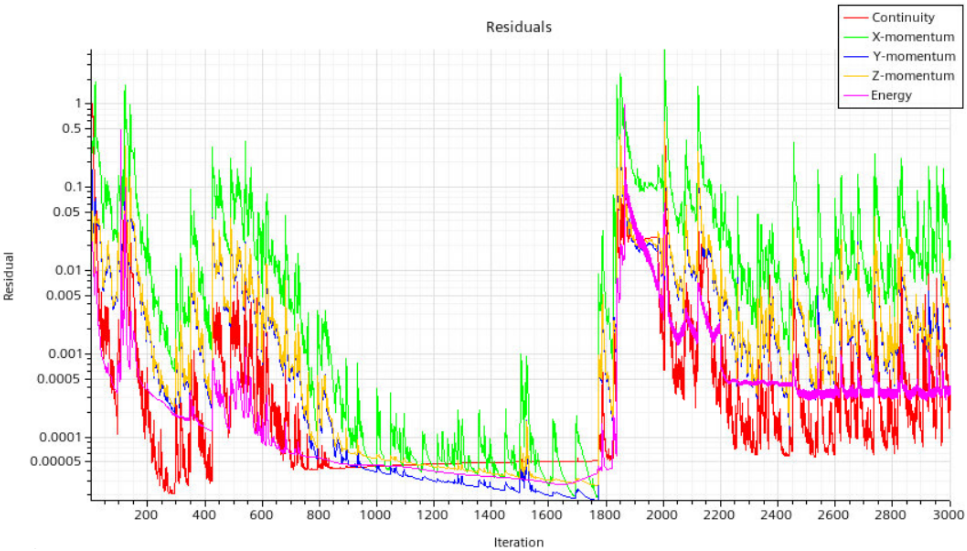

Figure 6.1: The residual plot for the numerical simulation.

The pressure distribution along the screw shows a decreasing trend in the flow direction, as shown in Figure 6.2. Instead of increasing towards the outlet due to the back pressure imposed by the accumulator, the pressure decreases, indicating that the pressure boundary conditions or the flow modeling are not correctly set up.

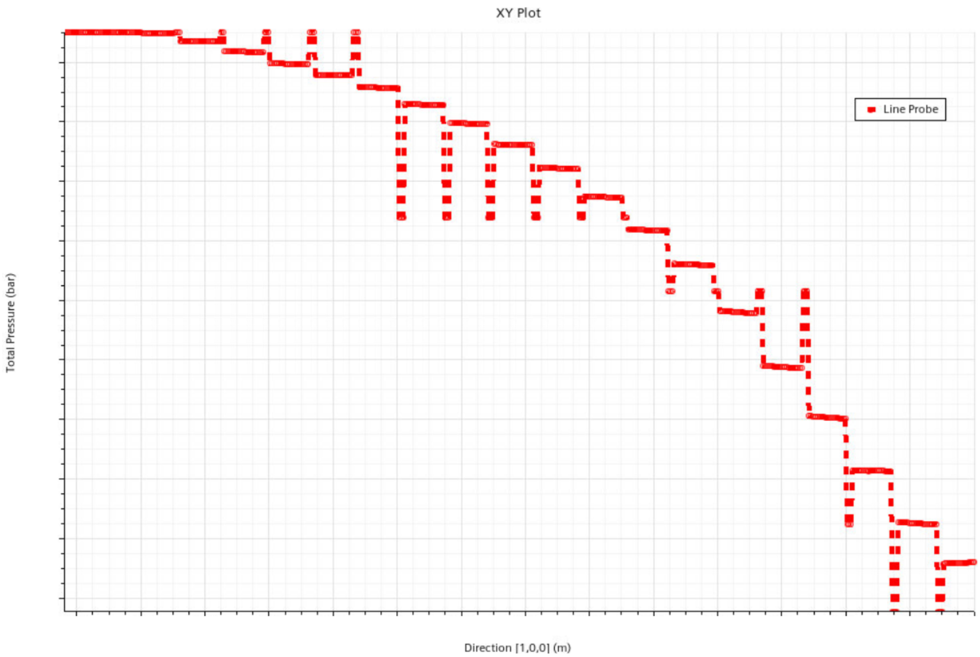

Figure 6.2: Pressure along the screw.

The mass flow rate stabilizes after an initial phase, see Figure 6.3, apart from short peaks that occur at the same time as increased residuals. These peaks therefore appear to be related to numerical instability rather than changes in the physical flow. When different pressure boundary conditions were applied, the mass flow rate stayed at the same value. This insensitivity to changes in pressure settings further suggests that the numerical model does not correctly capture how pressure influence the mass flow rate.

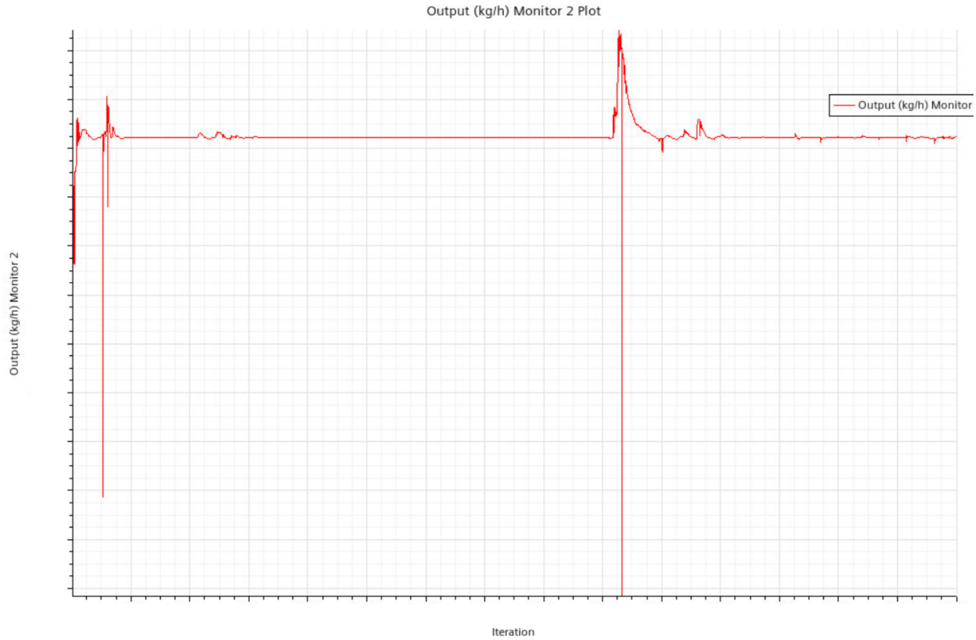

Figure 6.3: Mass flow rate from simulation model.

6.2 Parameter Trends

To identify general trends in how the design parameters influence the mass flow and the power consumption separately, the analytical model was evaluated across the defined design space. By comparing the calculated output parameters values for the different input parameter combinations, the direction of influence for each parameter could be identified. For the mass flow rate, the results show that higher values are obtained when the clearance and axial flight width is minimized, while the screw core diameter, axial channel width and flight height is maximized, see Equation (6.1). For power consumption, a different trend is observed. The power consumption is minimized when the clearance, axial flight width and flight height is maximized while the screw core diameter and axial channel width is minimized. See Equation (6.2).

$$\dot{m}_{max} = \delta_{f,min} + e_{axial,min} + D_{s,max} + W_{axial,max} + h_{f,max} \tag{6.1}$$

$$P_{w,min} = \delta_{f,max} + e_{axial,max} + D_{s,min} + W_{axial,min} + h_{f,max} \tag{6.2}$$

6.3 Response Surface Results

From the DOE two response surfaces were established, which will be presented below along with parameter influence and residual analysis. The response surfaces were based on the regression models presented below.

6.3.1 Regression Models

From the DOE created in the develop phase a response surface was created. This response surface gave an indication of how the geometrical parameters influence the mass flow and energy consumption, which lays ground for the framework. This representation allows direct evaluation of the mass flow rate and power consumption for the given geometrical parameters. The regression equation for the mass flow rate is seen in Equation (6.3), and the regression equation for the energy consumption is seen in Equation (6.4) where non relevant parameters were omitted due to selecting Stepwise regression.

$$\begin{aligned} \dot{m} = 29.14 &- 1140.6 D_s - 703.6 W_{\text{axial}} + 321 e_{\text{axial}} \\ &- 11552 h_f - 7996 W_{\text{axial}}^2 + 36765 D_s W_{\text{axial}} \\ &+ 415870 D_s h_f - 8369 W_{\text{axial}} e_{\text{axial}} + 341138 W_{\text{axial}} h_f \\ &- 105415 e_{\text{axial}} h_f \end{aligned} \tag{6.3}$$

$$\begin{aligned} P_w = &- 51 + 114624\,\delta_f - 11161\,D_s - 563\,W_{\text{axial}} + 24158\,e_{\text{axial}} + 16365\,h_f \\ &+ 4728762\,D_s^2 - 219517\,W_{\text{axial}}^2 + 183847863\,h_f^2 \\ &- 49920109\,\delta_f D_s + 389720526\,\delta_f h_f + 719136\,D_s W_{\text{axial}} \\ &- 5643779\,D_s e_{\text{axial}} - 44492242\,D_s h_f + 1750125\,W_{\text{axial}} e_{\text{axial}} \\ &- 2373403\,W_{\text{axial}} h_f + 15460804\,e_{\text{axial}} h_f \end{aligned} \tag{6.4}$$

6.3.2 Parameter Influence

From the response surface analysis in Minitab, Pareto charts of the standardized effects were generated, showing the relative influence of each design parameter on the mass flow and power consumption. The results are presented in Figures 6.4 and 6.5.

The Pareto charts include main effects, interaction effects, and quadratic effects. Main effects is represented by a single letter. Terms with two different letters represent interaction effects between parameters, indicating that the influence of one parameter depends on the level of another. Terms with repeated letters represent quadratic effects, indicating non-linear relationships between the parameters and the response. For both mass flow and power consumption, several interaction effects are present, although their magnitude is generally smaller than the main effects.

For the mass flow, the flight height shows the largest influence, followed by the axial channel width and the screw diameter. The axial flight width has a relatively small influence, while the clearance does not show a notable effect within the investigated parameter interval.

For the energy consumption, the screw diameter has the largest influence, followed by the flight height and the axial channel width. The most significant interaction effect is observed between the screw diameter and the flight height. The axial flight width has a comparable influence to this interaction effect, while the clearance shows the smallest main effect.

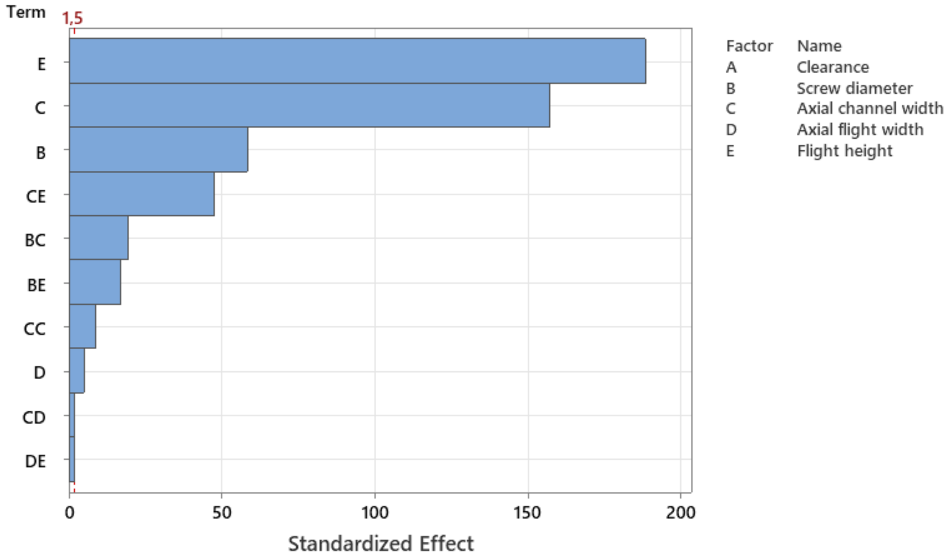

Figure 6.4: Pareto chart of the standardized effects of mass flow.

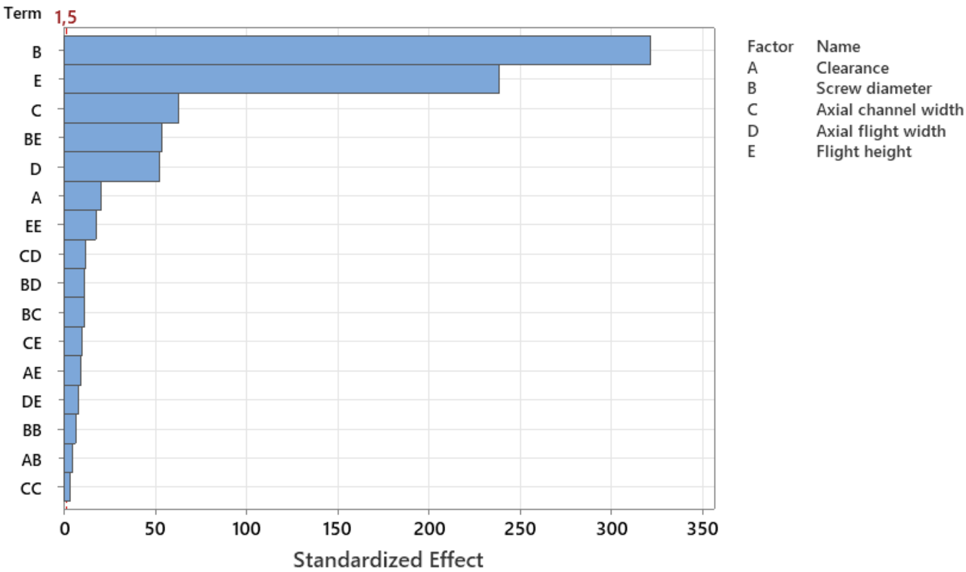

Figure 6.5: Pareto chart of the standardized effects of energy consumption.

In addition to the Pareto charts, factorial plots were used to visualize how the output changes with variations in each parameter. The main effect plots, Figure 6.6 and 6.7 show the direction of influence, where the slope of each line indicates whether an increase in a parameter leads to an increase or decrease in the response. The results show that mass flow increases with increasing screw diameter, axial channel width, and flight height, while it decreases slightly with increasing axial flight width. For power consumption, the plots show that increasing screw diameter and axial channel width leads to increased power consumption, while increasing clearance, axial flight width and flight height reduces power consumption.

The factorial interaction plots, Figure 6.8 and 6.9 further support the results from the Pareto analysis. Most of the interaction lines are close to parallel, indicating that the interaction effects are relatively weak compared to the dominant main effects. Together, the Pareto and factorial plots provide a consistent understanding of the parameter influence, where the Pareto charts describe the relative importance of each parameter and the factorial plots confirm the direction of influence.

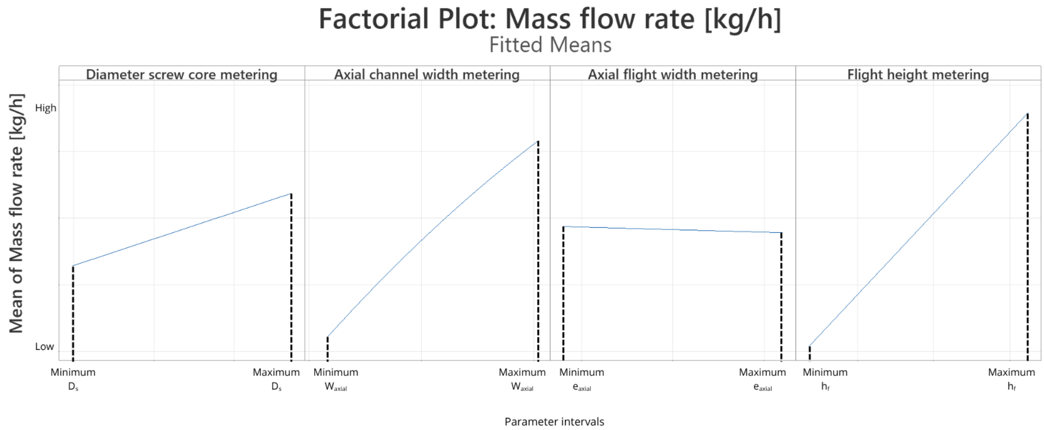

Figure 6.6: Main effect plot for mass flow rate.

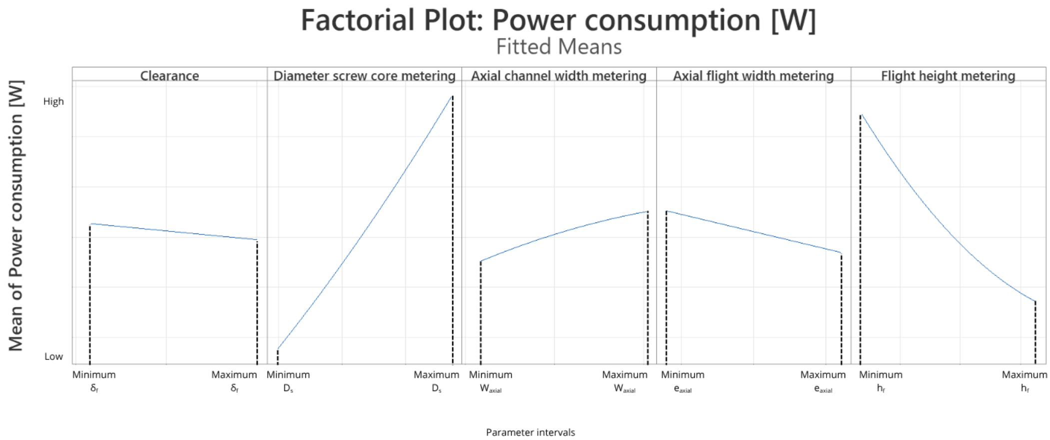

Figure 6.7: Main effect plot for power consumption.

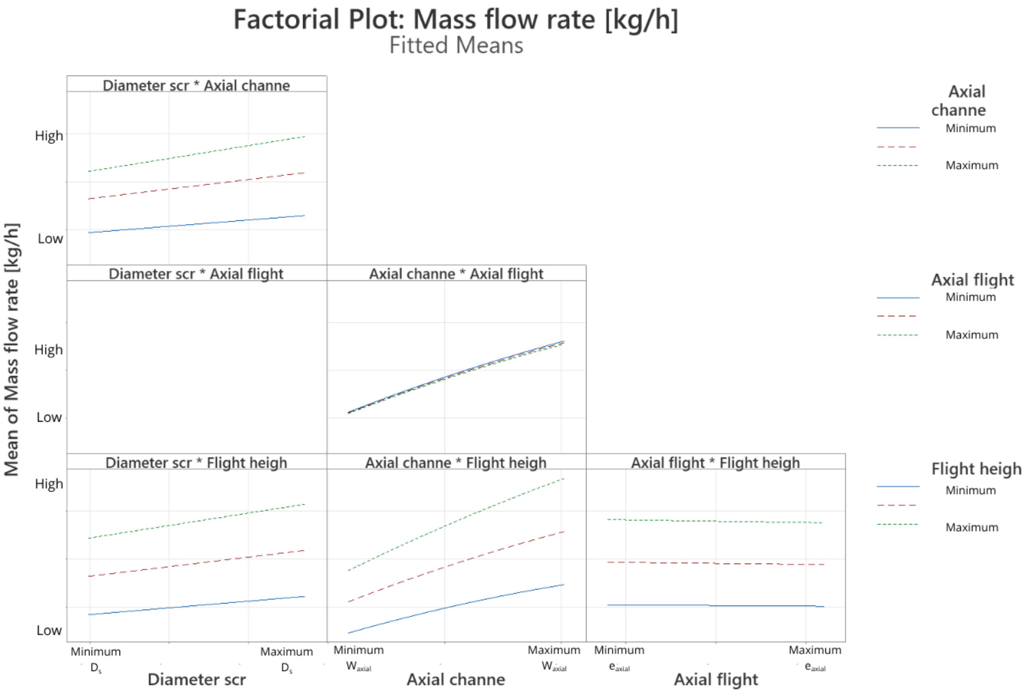

Figure 6.8: Factorial interaction plot for mass flow rate.

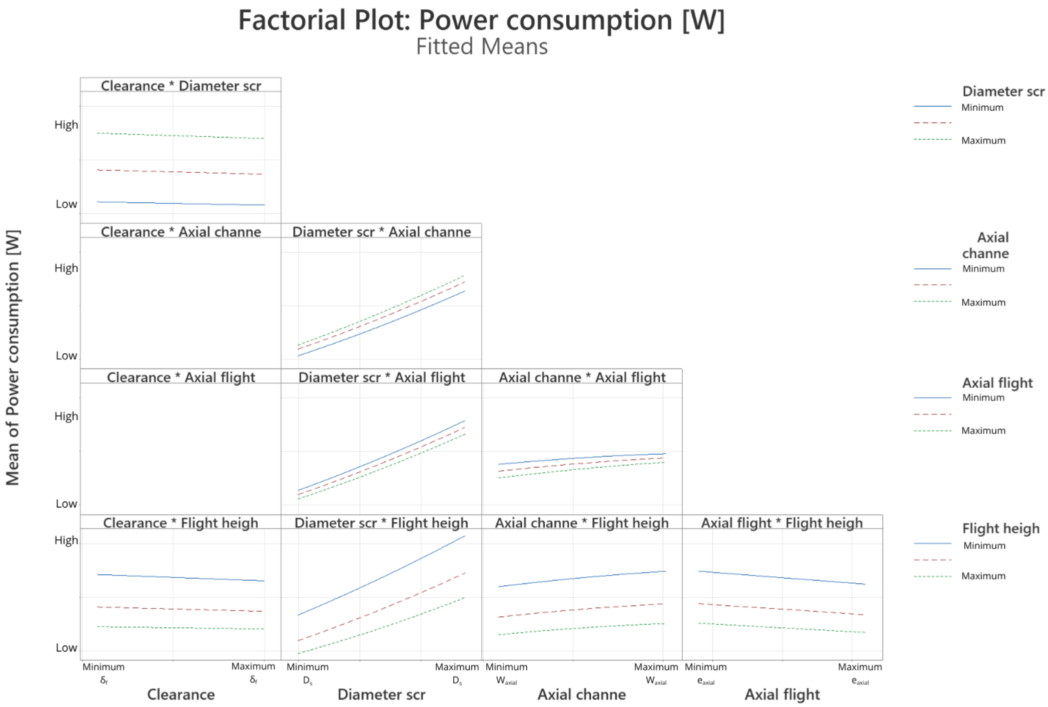

Figure 6.9: Factorial interaction plot for power consumption.

6.3.3 Residual Analysis

Residual plots were used to assess the validity of the regression models for both mass flow and power consumption.

For both models, the residuals plotted against the fitted values, shown in Figures 6.10 and 6.11, the residuals are spread around zero without any clear pattern. This means that the models do not show any obvious systematic errors and can be considered reasonable.

The normal probability plots, shown in Figures 6.12 and 6.13, suggest that the residuals are approximately normally distributed for both responses. Minor deviations from linearity are present, particularly at the extremes for the mass flow model, but these are considered acceptable within the context of the study.

Since the regression models are based on analytical calculations rather than experimental data, no significant deviations are expected. The residual analysis therefore primarily serves as a consistency check of the models.

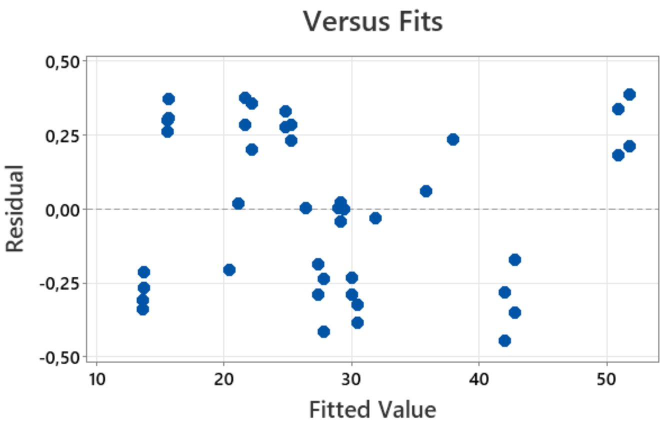

Figure 6.10: Residuals versus fitted values for the regression model of mass flow.

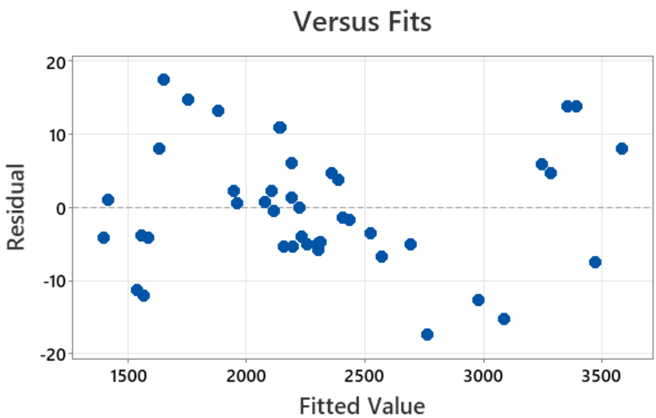

Figure 6.11: Residuals versus fitted values for the regression model of power consumption.

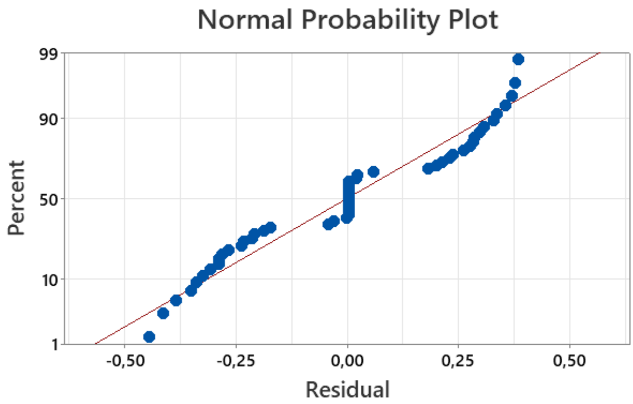

Figure 6.12: Normal probability plot of the residuals for the regression model of mass flow.

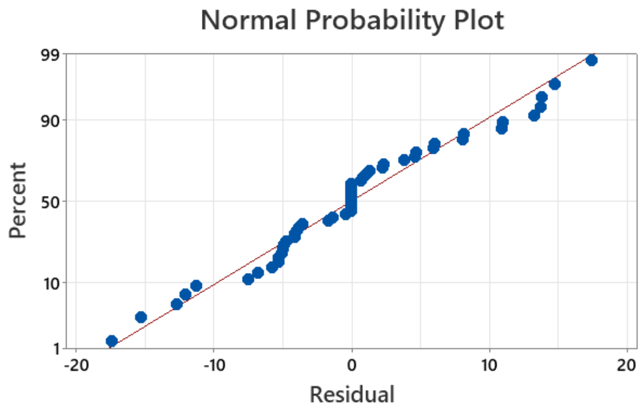

Figure 6.13: Normal probability plot of the residuals for the regression model of power consumption.

The model summaries of the response surfaces indicate that the models fit the data well. The coefficient of determination (R^2) for the mass flow rate is 99.94%, which means that the model describes the data well. The standard deviation for the mass flow rate is 0.272 kg/h, which is small compared to the overall flow rate and only indicates small errors. For the power consumption, the R^2 value is 99.98% and the standard deviation is 9.14 W, which is small compared to the overall power consumption. This also indicates that the model represents the data well. The high R^2 values are expected, since the models are based on analytical calculations rather than experimental data.

6.4 Response Optimization

From the response surface optimization, multiple response predictions were obtained. The predictions illustrates the expected trade-offs between maximized or targeted mass flow rate and minimized power consumption, and the optimized solution represents a balance between these two objectives.

The red vertical lines indicate whether the optimal value of each geometrical parameter is located at the lower or upper limit of the defined parameter interval. Parameters at the bounds suggest that the optimum lies at the edge of the explored design space.

The composite desirability summarizes how well the solution satisfies both optimization objectives. A high composite desirability indicates that a good compromise between mass flow rate and power consumption has been achieved.

Figure 6.14 shows the response optimization for maximizing mass flow rate while minimizing power consumption. The results indicate that the optimal solution places most geometrical parameters at the upper limit of their respective intervals, except the screw diameter which is located at its lower limit. The desirability value for power consumption is relatively high, showing that the optimized solution achieves a low energy usage close to the desired minimum. The desirability value for mass flow rate is lower, which indicates that maximizing mass flow rate is partly limited by the requirement to keep power consumption low. The composite desirability of 0.8248 represents the overall quality of the solution when both objectives are considered simultaneously. This value indicates that the optimization results in a balanced compromise, where power consumption is prioritized slightly more strongly than mass flow rate, while still achieving a high overall performance.

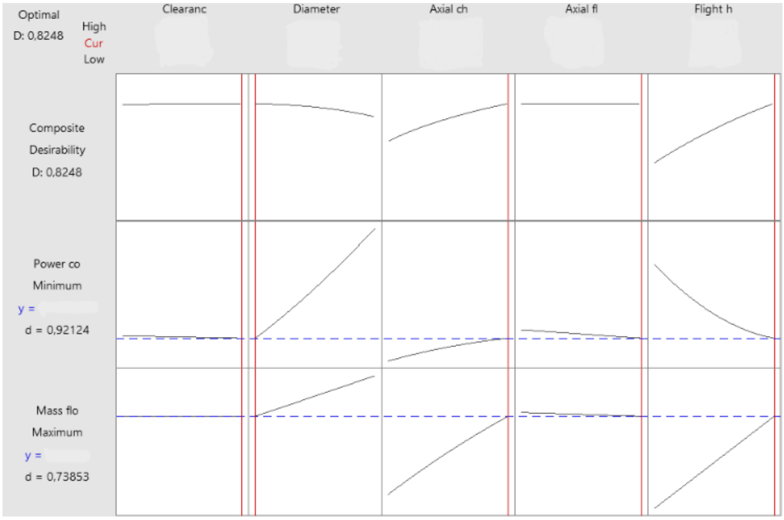

Figure 6.14: Multiple response prediction for maximizing mass flow rate and minimizing power consumption.

Figure 6.15 shows the response optimization where the power consumption is minimized and the mass flow rate is defined using a target value corresponding to the highest volume throughput. The suggested design resulted in a high composite desirability of 0.9688, indicating that the optimization meets both objectives well. The desirability value for the mass flow rate is slightly higher than for the power consumption. This is explained by the higher weight factor used for mass flow rate, causing the optimization to prioritize solutions close to the specified target value for the mass flow rate. The red vertical lines indicate that the screw diameter and axial channel width are set to their minimum values within the defined intervals. The axial flight width is also located in the lower part of its interval. Clearance and flight height on the other hand, are set at their maximum values.

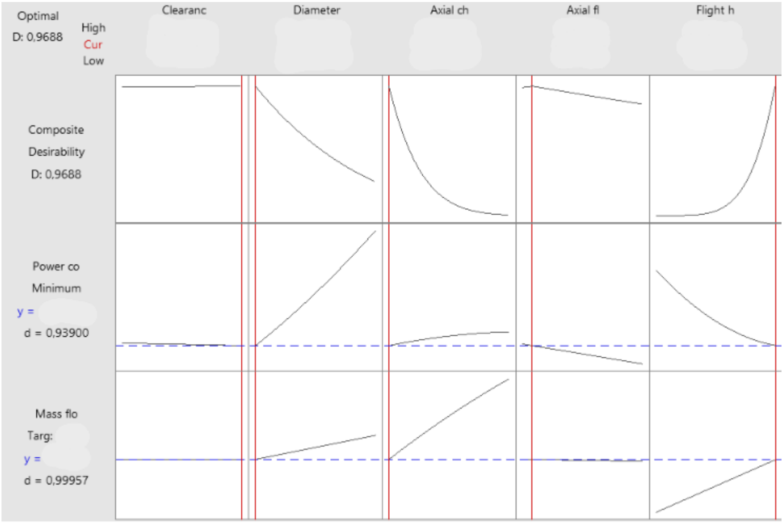

Figure 6.15: Multiple response prediction for minimizing power consumption and targeting the mass flow rate towards the highest volume.

Figure 6.16 shows the response optimization where the power consumption is minimized and the mass flow rate is defined using a target value corresponding to the medium volume throughput. The optimization results in a composite desirability of 0.8913, indicating a good overall compromise between the two objectives. The desirability for mass flow rate is high, approximately 0.99, while the desirability for power consumption is lower, approximately 0.80. This shows that achieving the target mass flow rate is prioritized, which is expected since a higher weight factor was applied to mass flow rate. The red vertical lines indicate that clearance and axial flight width are set to their maximum values, while the screw diameter is minimized. The axial channel width and flight height are located in the lower part of their respective intervals.

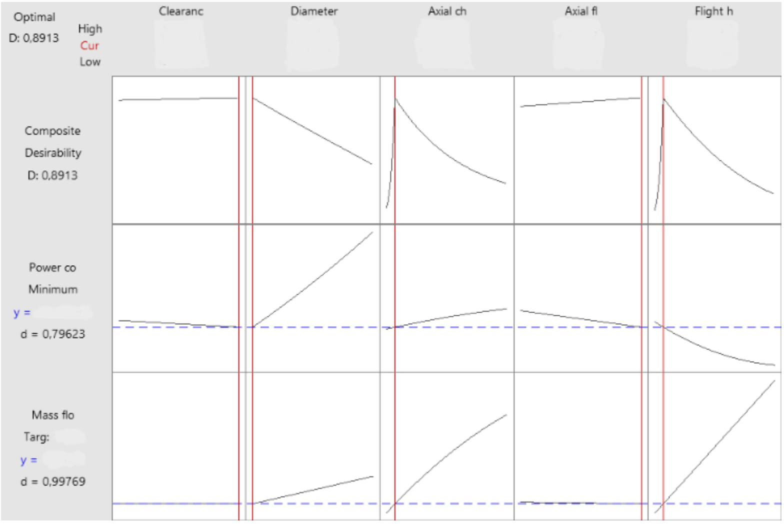

Figure 6.16: Multiple response prediction for minimizing power consumption and targeting the mass flow rate towards the medium volume.

Figure 6.17 shows the response optimization where the power consumption is minimized and the mass flow rate is defined using a target value corresponding to the low volume throughput. The composite desirability is 0.4955, indicating that the optimization does not provide a suitable solution for this case. The desirability for the mass flow rate is low, approximately 0.32, while the desirability for power consumption is higher, approximately 0.78. This shows that, within the defined parameter intervals and modeling assumptions, the required low material throughput cannot be achieved. The optimized solution produces approximately 53% more material than desired, suggesting that the current design space does not adequately cover the low volume throughput and may need to be extended. Regarding the geometrical parameters, the red vertical lines follow the opposite trend compared to maximizing mass flow rate, see Equation (6.1).

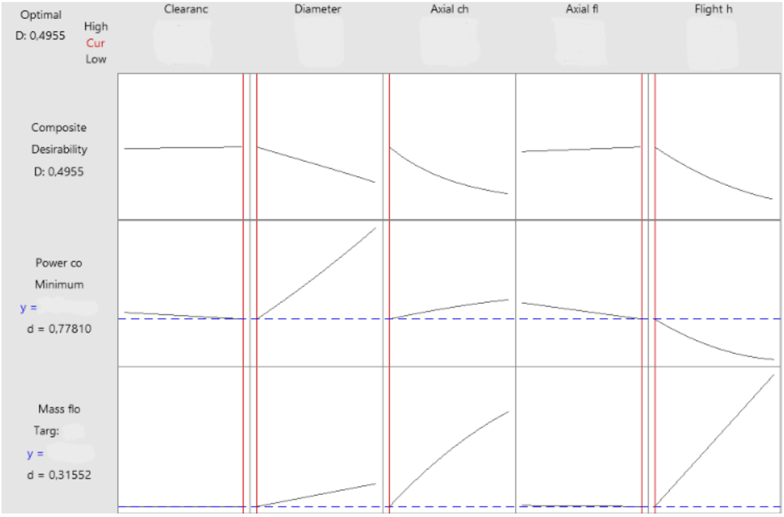

Figure 6.17: Multiple response prediction for minimizing power consumption and targeting the mass flow rate towards the low volume.

To further illustrate the outcome of the response surface optimization, the geometries of the screw concepts are shown in Figures 6.18-6.21. Each concept corresponds to a specific optimization case and reflects how the geometrical parameters are adjusted to meet different performance objectives.

Figure 6.18 shows the screw concept obtained when maximizing mass flow rate while minimizing power consumption. In this case, most parameters are driven towards their extreme values, resulting in a geometry that prioritizes high throughput while maintaining a relatively low power demand according to the model.

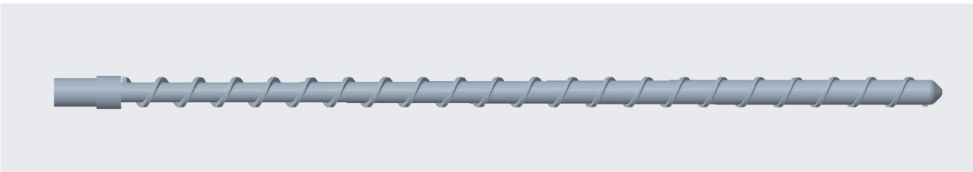

Figure 6.18: Optimized screw geometry for maximizing mass flow rate and minimizing power consumption.

Figures 6.19-6.21 present the screw concepts obtained when minimizing power consumption while targeting the required mass flow rate for high, medium and low volume, respectively. The screw concepts for the targeted mass flow rates are relatively similar in appearance, while they differ to a greater extent from the concept aimed at maximizing the mass flow rate.

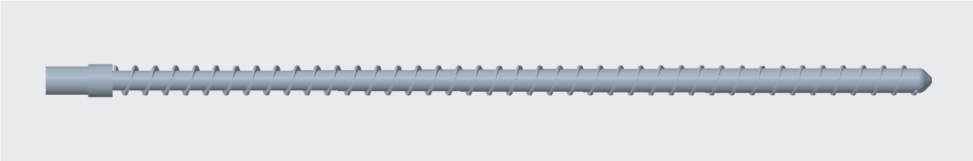

Figure 6.19: Optimized screw geometry for targeted mass flow rate (high volume) and minimized power consumption.

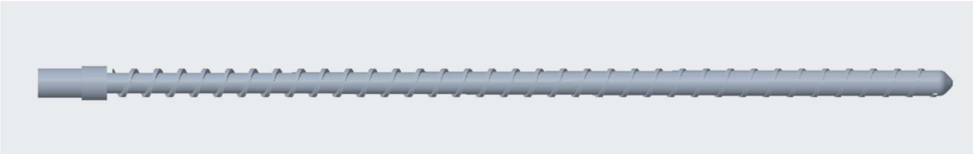

Figure 6.20: Optimized screw geometry for targeted mass flow rate (medium volume) and minimized power consumption.

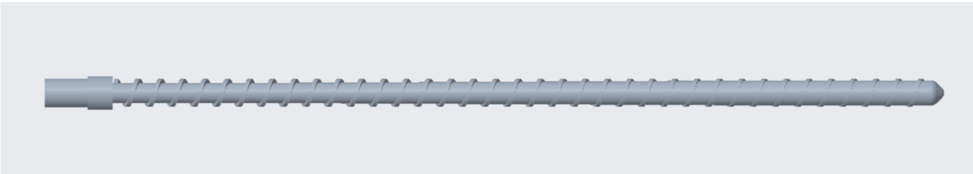

Figure 6.21: Optimized screw geometry for targeted mass flow rate (low volume) and minimized power consumption.

Figure 6.22 shows a cross-sectional comparison of the different screw concepts, highlighting the geometrical differences between the designs, all focusing on minimizing power consumption. The top cross-section corresponds to the concept for maximizing mass flow rate and differs the most from the other designs, mainly due to a larger axial channel width.

Below this, the second cross-section represents the concept for the targeted mass flow rate for the high volume. The two cross-sections following correspond to the concepts for the medium volume and low volume. These two designs are similar in appearance, although differences in axial channel width and flight height can be observed, as shown in Figures 6.16 and 6.17. The main difference between these concepts and the concept for the maximum targeted mass flow rate is a smaller axial flight width and a larger flight height.

The bottom cross-section represents the current screw design, which is shorter and has a slightly larger core diameter compared to the optimized concepts.

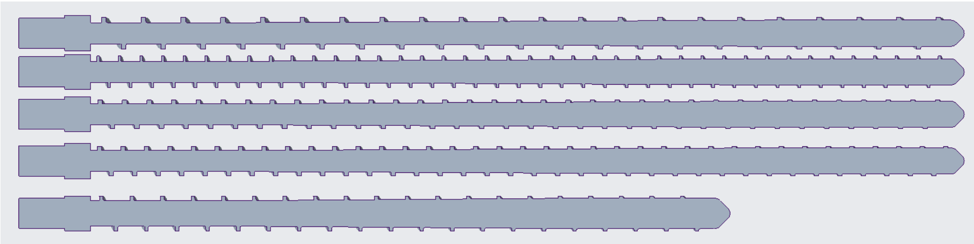

Figure 6.22: Cross-sectional comparison of the optimized screw geometries corresponding to Figures 6.18-6.21. They are presented in the same order as above, with the bottom cross-section representing the current screw design.

7 Framework

The aim of this thesis is not only to analyse the influence of screw geometry, but also to provide a structured approach for how these results can be used in practice. Based on the findings, two frameworks are proposed, see Figure 7.1 and 7.2.

The first framework describes the process of establishing an analytical model and a response surface for a given extrusion process. The process begins by defining the performance objective and identifying the limitations of the process. Based on these constraints, appropriate parameter intervals are defined. A DOE is then performed in Minitab to obtain the design points within the design space, based on the parameter intervals. Then the design points are inserted to excel with the analytical formulas for the process which then calculates the output values. The calculated output values are then used to construct a response surface model in Minitab, which can be used for further analysis and optimization.

The second framework describes how the already developed model can be used to guide screw design. The process begins by selecting the performance focus, such as maximizing mass flow, minimizing power consumption, or considering both objectives simultaneously. For single-objective cases, the design direction can be determined directly using the identified parameter trends, see Equation (6.1) and (6.2). These trends show how each parameter should be adjusted in order to improve the selected performance measure. However, process limitations may restrict the possibility to fully follow these trends. In such cases, Pareto or factorial charts can be used to prioritize the most influential parameters.

For cases where multiple objectives are considered, the parameter trends are not aligned, meaning that an increase in one performance measure may lead to a decrease in the other. In such cases, an optimization approach is required, where the desired balance between mass flow and power consumption is defined. The response surface model can then be used to determine a suitable compromise by setting target values or weighting the importance of each objective.

The resulting design should finally be evaluated to ensure that it is feasible within the defined parameter intervals and process limitations.

The second framework can be directly applied in cases where the response surface is representative of the process under consideration, such as for the studied Tetra Pak system. In such cases, there is no need to establish a new response surface. However, if the process conditions, limitations, or design space differ, the first framework should be applied in order to establish a new model before using the second framework for design decisions.

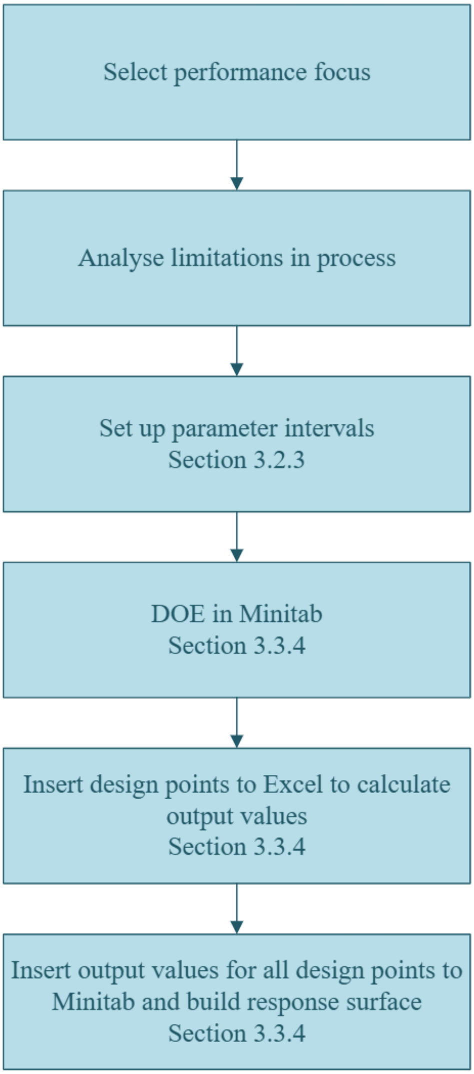

Figure 7.1: Framework 1: Establishment of analytical model and response surface.

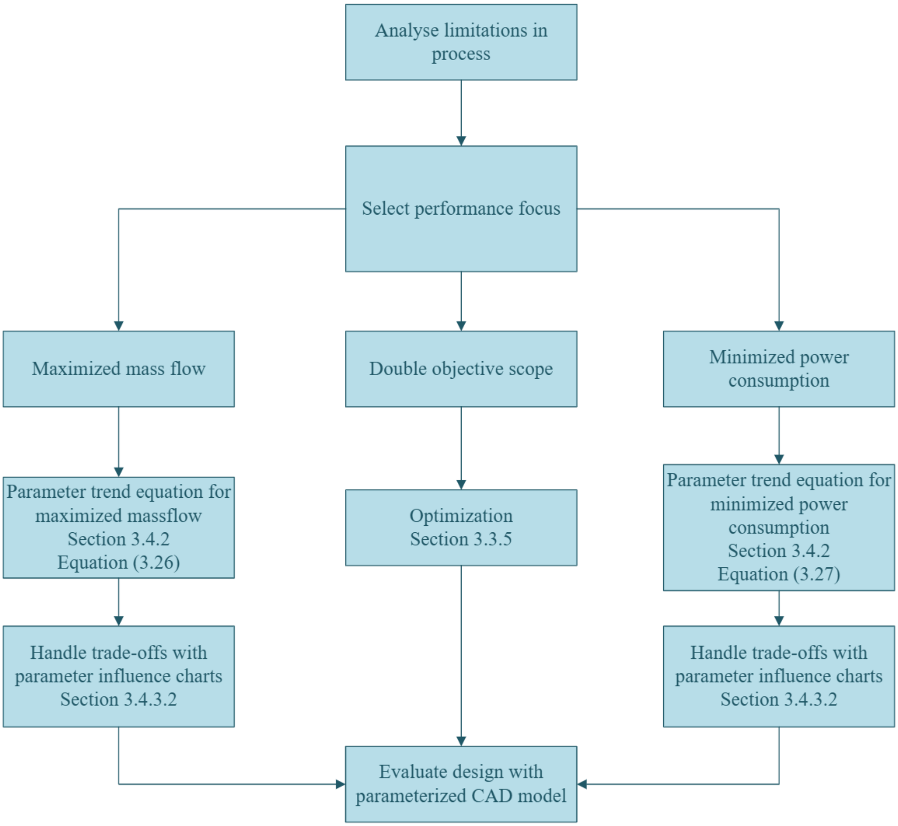

Figure 7.2: Framework 2: Usage of already designed model to guide screw design.

Using these frameworks for the multi-objective purpose to maximize mass flow rate while minimizing power consumption, the CAD model of the final optimized design proposal is shown above in Figure 6.18 under Section 6.4.

8 Discussion

This chapter discusses the results of the thesis in relation to the project objective of developing a structured framework for extrusion screw design based on geometrical parameters. The findings from the numerical model, analytical model and the optimization are analyzed in terms of validity, limitations, and practical relevance.

8.1 Numerical Simulation

The results of the numerical simulation work showed that a reliable simulation model could not be achieved within the time frame of this project. The simulation exhibited several fundamental issues, including convergence issues, unrealistic pressure behavior, and mass flow rates that were largely insensitive to changes in boundary conditions. These observations indicate that the numerical model was not suitable as a basis for design decisions.

One contributing factor was that the STAR-CCM+ model provided at the start of the project was incomplete and required significant additional setup. Completing and validating such a model requires advanced CFD knowledge, especially for extrusion processes where flow, pressure, temperature, and material behavior strongly influence each other. Despite multiple attempts to adjust boundary conditions, solver settings, and region definitions, the simulation remained numerically unstable and did not deliver expected physical behavior, such as pressure build-up due to accumulator back pressure.

Given these limitations, it was assessed that further development of the CFD model would require a level of expertise, validation effort, and time that exceeded the scope of the thesis. As a result, the decision was made to discontinue the numerical simulation track and instead focus on the analytical modeling approach.

The absence of a validated simulation model influenced the final scope of the project. With a fully functioning CFD model, it would have been possible to study detailed pressure and temperature variations along the screw, as well as local flow phenomena. These aspects had to be simplified or excluded in the analytical model. Nevertheless, the project still delivers a structured framework for extrusion screw selection based on the analytical model, which fulfills the main objective of the thesis. The simulation work therefore contributed primarily by defining limitations rather than by providing direct quantitative results.

8.2 Analytical Model

The analytical models used in this study provide a simplified representation of the extrusion process and are primarily used to evaluate how geometrical parameters influence mass flow rate and power consumption. The models are based on established theoretical expressions and describe the process in the metering section under a set of simplifying assumptions. While the model do not fully capture the complexity of the physical process, it enables a consistent and efficient analysis of parameter influence within the defined design space.

The results from the analytical models are therefore interpreted in terms of trends and relative differences, rather than as exact predictions of the real process. The following sections discuss the behaviour, validity and assumptions of the models for mass flow rate and power consumption.

8.2.1 Mass Flow Rate

The analytical model used to describe the mass flow provides a simplified but physically motivated representation of the extrusion process. The model is based on the balance between drag flow, driven by the rotation of the screw, and pressure-driven flow acting in the opposite direction. This balance says how the flow develops in the screw channel in the metering section and shows how changes in geometry affect the mass flow.

The results indicate that the analytical model captures the overall behaviour of the mass flow in a consistent way. The formulation of the model implies that the mass flow should increase with screw rotational speed, as the drag-driven flow is directly dependent on the screw rotation. To further verify this, the model was evaluated at several different rotational speeds and compared with the corresponding experimental results. This comparison showed that the model follows the same general trend as observed in the experiments, where the mass flow increases with increasing screw speed. In addition, the calculated mass flow matches well with the measured value at the operating point used for validation. This indicates that the model provides a good approximation of the process, not only at a single operating point, but also in terms of how the mass flow varies with screw speed. As a result, the model can be considered reliable for capturing the overall behaviour and for further analysis of the influence of the geometrical parameters.

The analytical model used to describe the mass flow is based on a number of simplifying assumptions, where each assumption reduces the complexity of the model but also influences its accuracy. It is therefore important to evaluate these assumptions and assess their impact on the results.

One of the simplifications in the model is the assumption of isothermal conditions. In reality, the extrusion process is not isothermal, as temperature varies along the screw due to viscous dissipation and heat transfer with the barrel. These temperature variations affect the viscosity of the polymer, which in turn influences the flow. In the analytical model, this complexity is reduced by assuming a constant temperature in the studied metering section, and the viscosity is instead represented through an average value, one by the flight and one by the screw core. Although this is a simplification, it is considered acceptable for this study, since the primary objective is to evaluate the influence of geometrical parameters rather than to predict absolute values with high precision.

As previously mentioned the viscosity is represented by one value by the screw core and another value at the screw flight. The model includes non-Newtonian behavior through the Cross-WLF viscosity model, and different viscosity values are used for the channel and the clearance region. This captures some of the variation in shear conditions within the screw. However, in reality, the viscosity depends continuously on the local shear rate, temperature and pressure, which vary along the entire length of the screw. This variation is not fully resolved in the analytical model, and the viscosity is therefore approximated using representative values. As a result, the model captures the overall behaviour of the flow, but not the detailed local variations.

The leakage flow over the flight clearance is also simplified in the model. Leakage is included through the correction factor, which provides an approximation of the backflow. However, the actual leakage flow depends on local pressure gradients, viscosity variations and the geometry of the clearance region. These effects vary along the screw and interact with each other in a complex way. In the analytical model, this behaviour is represented in a simplified form, which means that the magnitude and distribution of the leakage flow may not be captured exactly. Despite this, the inclusion of a leakage term allows the model to account for the dominant effect of backflow and thereby improves the physical realism compared to a purely drag-based model.

Another assumption in the model is the estimation of the pressure build-up along the screw. In this study, the change of pressure in the metering section is not directly measured, but instead approximated as a fraction of the total pressure build-up in the process, based on typical behaviour for conventional extrusion screws. In reality, the pressure distribution along the screw depends on the geometry, material properties and operating conditions. This means that the assumed pressure build-up represents a coarse approximation of the actual process. A more accurate determination of the pressure gradient would require experimental measurements, for example using pressure sensors placed along the barrel, or numerical simulations. Despite this limitation, the chosen approximation is considered sufficient for the purpose of this study, since it provides a consistent basis for comparing different geometrical configurations.

As a consequence of the simplifying assumptions in the model, deviations from the real process behaviour can be expected. While the analytical model captures the dominant mechanisms governing the flow, the simplified representation of temperature, viscosity, leakage and pressure distribution affects the accuracy of the predicted mass flow under varying operating conditions. This can be observed when analyzing the relationship between mass flow and screw rotational speed. Although the model agrees well with the experimental results at the operating point used for validation, the calculated curve shows a slightly flatter trend compared to the experimental data, see Figure 5.1 and 5.2. This indicates that the model tends to overestimate the mass flow at lower rotational speeds. Despite this deviation, the model is considered sufficiently accurate for the purpose of this study.

8.2.2 Power Consumption

The analytical model used to estimate the power consumption provides a simplified representation of the energy required to drive the extrusion screw and feed the material forward at the chosen speed. The model is based on established analytical expressions for shaft power input, where the energy demand depends on parameters such as screw geometry, rotational speed and melt viscosity. To represent the operating conditions of the process, the model assumes a pressure-restricted system corresponding to closed discharge. This reflects the presence of the accumulator, which imposes a back pressure and increases the mechanical load on the screw.

When the analytical results were compared with experimental data in the Develop phase, it was observed that the model did not match the absolute values of the measured power consumption. The calculated values are lower than the experimental results, about half the size, indicating that the model underestimates the required power. This shows that the model cannot be used to predict exact power consumption levels for the process.

The deviation between calculated and measured values can be explained by several simplifying assumptions in the model. One important limitation is that leakage over the screw flights is neglected in the formulation. In reality, some backflow always occurs, which increases shear and leads to additional energy losses. Furthermore, the model does not include mechanical losses in the system, such as inefficiencies in the motor, gearbox, bearings and the screw itself. These effects contribute to a higher real power demand compared to the analytical prediction. The model also assumes idealized flow behavior in the metering section, meaning that variations in shear, pressure and temperature are not fully represented. In reality, these effects increase the resistance to flow and therefore the required power. As a result, the analytical model underestimates the actual energy demand.

Despite these deviations, the model captures how the power consumption responds to changes in the geometrical parameters. The predicted trends are consistent and can therefore be used to analyze how different design choices influence the energy consumption. One notable result is that the model suggests that increasing the clearance reduces the required power. This is a consequence of the simplified formulation, where reduced shear leads to lower flow resistance. In practice, however, increased clearance also leads to higher leakage and reduced efficiency, which are not captured by the model. The clearance between the flights and the barrel must therefore remain limited, since a larger gap increases leakage and negatively affects process performance. In this study, the clearance is constrained by the defined parameter intervals and can be interpreted as a controlled gap between the screw and the barrel. This becomes particularly important when comparing power consumption with mass flow rate and will be further discussed in Section 8.3 in relation to the identified parameter trends.

Overall, the analytical model for power consumption should be interpreted as a tool for understanding trends and relative differences rather than providing exact predictions. Although the absolute values deviate from experimental results, the model captures the main relationships between geometry and energy demand. This makes it suitable for comparing different design alternatives and supports the overall analysis of trade-offs within the developed framework.

8.3 Parameter Trends

The parameter trends, Equation (6.1) and (6.2) presented in section 6 Deliver, show a clear relationship between the geometrical parameters and the process performance. For mass flow, the results indicate that an increase in screw diameter, axial channel width and flight height, and a decrease in clearance and axial flight width leads to higher mass flow rate. For power consumption, the trend is that a decrease in screw diameter and axial channel width, and an increase in clearance, axial flight width and flight height gives a lower power consumption.

These trends show that geometrical parameters, in most cases, influence the mass flow and power consumption in different directions. Parameters that increase the mass flow usually leads to an increase in power consumption as well. While parameters that reduce power consumption usually decrease the mass flow rate, which shows that there's a conflict between the output parameters. But there is one exception, which is the flight height. That parameter theoretically both increases the mass flow rate and decreases the power consumption, when being increased. A larger flight height means a deeper channel, which reduces the shear of the material. Lower shear can reduce the required mechanical work, which can explain the decrease in power consumption. At the same time, the larger channel volume allows more material to be transported, which explains the increase in mass flow. However, this does not capture the full behaviour of the real process. In the physical process, an increased flight height would also affect things like pressure build-up, mixing and melting of the material. A deeper channel can make it harder to build up pressure, which can give a less stable process or poorer melting. These effects are not included in the analytical model, which only describes the metering section under simplified conditions. This means that the result should be interpreted with some caution. The model shows a clear trend, but in reality, increasing the flight height will not necessarily improve both mass flow and power consumption at the same time.

From a physical perspective, the trends observed for mass flow are in line with what is expected from extrusion theory. An increased screw diameter, channel width and flight height all contribute to a larger flow channel, which increases the drag-driven transport of material. Similarly, a reduced clearance limits the backflow through the leakage region, resulting in a higher net forward mass flow. These trends can therefore be considered physically reasonable.

For power consumption, some of the trends are also intuitive. An increase in screw diameter and channel width leads to a larger volume of material being sheared and transported, which increases the required mechanical work and therefore the power consumption. In this sense, the increase in power consumption for these parameters is consistent with the increased mass flow. However, not all observed trends are equally intuitive. In particular, the result that an increased clearance leads to a reduction in power consumption requires further consideration. From a physical standpoint, this behaviour may seem counterintuitive, as a larger clearance increases the leakage flow, which reduces the efficiency of the material transport. In a real extrusion process, this loss of efficiency would typically require additional mechanical work to maintain the same throughput. The explanation for this behaviour can be found in how the clearance is represented in the analytical model. The clearance does not appear directly in the power consumption expression, but instead influences the result indirectly through geometrical quantities such as the barrel diameter and the helix angles. As the clearance increases, these parameters change in a way that reduces the calculated power requirement in the model. At the same time, the model does not account for the additional energy losses associated with increased leakage flow. This means that the observed trend for clearance is primarily a consequence of the structure of the model, rather than a reflection of the physical reality. In reality, the influence of clearance is expected to be more complex, where increased leakage may reduce the efficiency of the process and potentially increase the required power.

Overall, the parameter trends provide a consistent picture of how the geometrical parameters influence the process performance, but the interpretation of individual parameters must be made with consideration of the assumptions in the analytical model. In particular, parameters that are only indirectly represented in the model, such as the clearance, require careful evaluation when translating the results to practical design decisions.

8.4 Parameter Influence

The parameter influence analysis provides insight into how strongly each geometrical parameter affects the output parameters. While the parameter trends describe the direction of the influence, the Pareto charts and factorial plots show how large the influence of each parameter is relative to the others.

For the mass flow, the flight height, axial channel width and screw diameter show the largest influence, while the axial flight width has a smaller effect and the clearance has very limited influence within the studied interval, which is why it is not included in the Pareto chart, Figure 6.4. This is in line with what can be expected physically. Parameters that directly affect the channel geometry, such as channel width and flight height, have a strong impact on how much material can be transported through the screw. The screw diameter also influences the overall flow capacity, which makes these parameters dominant for the mass flow.

The relatively low influence of clearance on the mass flow is also reasonable within the studied interval. The leakage flow is small compared to the overall channel flow, which explains why the clearances influence is small in the analysis. However, an additional observation from the analysis is that the influence of the clearance depends on its absolute value. Within the investigated range, the clearance has only a minor effect on the mass flow, but when increasing the clearance to larger values, the sensitivity increases. This means that the same absolute change in clearance can have a larger impact at higher values than at lower ones. From a practical perspective, this suggests that small variations in clearance may have limited impact as long as the clearance remains small. However, if the clearance becomes larger, the same variation can have a more significant effect on the flow. At the same time, this behaviour is based on the analytical model, and the real process may be more sensitive due to leakage flow and material behaviour that are not fully captured.

For the power consumption, the screw diameter, flight height and axial channel width again show the largest influence, see Figure 6.5. This is consistent with the fact that these parameters affect both how much material is being processed and the shear conditions in the flow. Increasing these parameters generally means that more material is transported and that the material experiences higher shear in total, which increases the mechanical work required.

From a practical perspective, the difference in parameter influence is important when considering design decisions. Since some parameters have a significantly larger effect than others, it means that the design process should focus primarily on those parameters. However, this must be balanced with the trade-offs identified earlier, as the most influential parameters also tend to create the strongest conflict between mass flow and power consumption.

Overall, the parameter influence analysis provides a consistent picture of which parameters are most important in the model. The results are generally in line with physical expectations, but the interpretation should always take into account the simplifying assumptions.

8.5 Response Surface & Optimization

The response surface models show a good fit to the data, as indicated by the high R^2 values, presented under Section 6.3.3, and the residual plots, see Figure 6.10 and 6.11. Since the response surfaces are based on analytically calculated data rather than experimental measurements, the high R^2 values mainly show that the models represent the analytical equations used in this study.

The response surface optimization illustrates how mass flow rate and power consumption interact within the defined design space. The optimization results should not be interpreted as exact solutions for the real extrusion process, but rather as indications of how the analytical model responds to changes in the geometrical parameters. In this way, the optimization highlights trends and trade-offs rather than providing final screw designs.

The cross-sectional comparison of the CAD-models in Figure 6.22, highlights how the screw geometries are influenced by the different optimization objectives. The design aimed at maximizing mass flow rate differs the most from the other concepts, primarily through a larger axial channel width, which reflects the trend described in Equation (6.1).

In contrast, the designs targeting specific mass flow rates are the result of a multi-objective optimization, where the mass flow is constrained to a target value while the power consumption is minimized. As these objectives are governed by separate parameter trends, see Equation (6.1) and (6.2), the resulting geometries represent a compromise between the two. This is reflected in the reduced axial channel width and adjusted flight height compared to the maximum mass flow design, balancing the required throughput with reduced energy demand.

For the low volume throughput, the optimization was unable to reach the target mass flow within the defined design space. The optimized solution produced about 53 % more material than desired, indicating that the parameter intervals are not sufficient to achieve lower flow rates. This explains why the screw concept for the low volume differs only slightly from the medium volume, as only minor geometric changes are possible within the current limits, see Figure 6.22. The observed geometrical variations illustrate how the optimization balances competing parameter trends and how the design space limits influence the resulting screw geometries.

Overall, the response surface optimization should be seen as a support tool for understanding parameter behavior and trade-offs. Together with engineering judgment and knowledge of the full extrusion process, the results provide guidance for screw design within the developed framework rather than exact design solutions.

8.6 Framework

The proposed framework provides a structured way of designing an extrusion screw based on the identified relationships between geometry and process performance. Rather than focusing on individual parameters, the framework links the parameter trends and parameter influence, and show how these should be considered together when making design decisions.

The framework is based on the results obtained in this study, where clear trends and conflicts between mass flow and power consumption were identified. By first analysing the direction of the parameter influence, and then considering how strongly each parameter affects the responses, the framework gives a logical order for how to approach the problem. This makes it easier to understand which parameters should be adjusted and which trade-offs that needs to be done.

The framework is particularly useful in cases where the process conditions and design space are similar to those studied in this thesis. In such cases, the developed response surface can be used directly, and the framework can be applied without the need to perform a new DOE, see Figure 7.2.

However, the applicability of the framework is limited by the assumptions made in the model and the defined parameter intervals. If the process conditions, material properties or geometrical constraints differ, the relationships identified in this study may no longer be valid. In such cases, a new analysis would be required, following the steps outlined in the first framework, see Figure 7.1.

Another important limitation is that the model focuses on the metering section and does not account for other aspects of the extrusion process, such as melting and mixing behaviour. This means that the framework should not be used as a complete design method, but rather as a decision-support tool for evaluating geometrical parameters within the studied scope. Despite these limitations, the framework provides a practical and systematic way of linking analytical results to design decisions. By making the trade-offs between different objectives clear, it helps guide the design process and reduces the need for trial-and-error based approaches.

8.7 Limitations & Future Work

The response surface and optimization results are based on a simplified analytical model, which introduces several limitations. The model only considers the metering section of the screw and does not include important aspects such as melting, mixing, temperature variations and pressure build-up along the full screw length.

The analytical model for power consumption introduces further simplifications. A limitation of the power consumption model is that it cannot accurately represent the actual energy demand, as the model consistently underestimates the measured values. This is probably due to the simplified representation of the flow, where effects such as local shear variations and energy losses are not fully included. Furthermore, the model may suggest parameter trends that do not fully reflect the physical process. This was observed for the clearance, where increased values reduce the calculated power despite increased leakage in practice. This shows that the model mainly reflects mathematical trends rather than the full physical behaviour of the extrusion process.

Based on these limitations, future work should focus on extending the analysis beyond the current assumptions. This could include incorporating more realistic representations of the process, such as temperature dependent viscosity and better descriptions of flow behavior in the metering section. Improving the analytical model in this way would provide a more reliable basis for design evaluation, especially when comparing different screw geometries. Furthermore, the analytical modeling approach could be extended to include the feed and transition sections of the screw. By implementing analytical models for these sections as well, including material transport in the feed section and melting and pressure build-up in the transition section, a more complete representation of the extrusion process could be achieved.

Future work could also focus on refining the power consumption model by including additional loss mechanisms, such as leakage effects and mechanical inefficiencies. Furthermore, calibrating the analytical model using updated experimental measurements would improve its accuracy. Since the validation in this study was based on previously collected data, performing new controlled experiments would provide a stronger basis for comparison before proceeding to further physical testing of new screw designs.

Future work could focus on developing a validated numerical simulation model for the extrusion process. With additional time and access to CFD expertise, the STAR-CCM+ model could be completed and systematically validated. This would involve a more careful setup of boundary conditions and material properties, as well as ensuring that the interaction between flow, pressure, and temperature is correctly represented so that the simulation model delivers a realistic process behavior.

A reliable CFD model would enable more detailed studies of pressure build-up, temperature distributions, and local flow phenomena along the screw, which were not possible within the scope of this thesis. Such information could be used to validate and refine the analytical model, as well as to extend the developed framework with simulation-based insights.

The parametric CAD model developed in this study also provides a structured foundation for future simulation work. Since the geometry is defined through adjustable parameters, it enables efficient variation of screw design and supports systematic evaluation of different configurations in a simulation environment. This reduces the effort required for model setup and makes it easier to integrate simulation into the developed framework.

In addition, future work could investigate a combined analytical-numerical approach, where the analytical framework is used for initial screening and design selection, while CFD simulations are applied to a smaller number of promising designs for deeper analysis. This would allow the strengths of both approaches to be utilized while managing complexity and computational cost.

9 Conclusion

This thesis has developed a structured framework for extrusion screw design based on geometrical parameters, with the aim of optimizing mass flow and energy consumption. The study combines analytical modelling and DOE to investigate how different geometrical parameters influence the process performance.

The analytical results show that the developed models capture consistent trends in how mass flow rate and power consumption respond to changes in screw geometry. A key observation is that most parameters influence the two performance measures in opposite directions, resulting in a clear trade-off between maximizing throughput and minimizing energy consumption. At the same time, the parameter influence analysis shows that not all parameters have equal importance, meaning that some parameters play a more critical role in design decisions than others.

The response surface modelling and optimization further illustrate how these relationships can be used to identify suitable parameter combinations within the defined design space. However, the optimization results also highlight that the model tends to push parameters towards their limits, which emphasizes the need to interpret the results in a practical context rather than as final design solutions.

The main contribution of this thesis is the proposed framework for extrusion screw design, which links the analytical results to practical decision making. The framework provides a structured approach for how to analyse parameter trends, evaluate their influence, and handle trade-offs between conflicting objectives. It can be directly applied to processes similar to the studied case, while also serving as a general methodology for analysing other extrusion systems. Although the analytical models are based on simplifying assumptions and are limited to the metering section, they provide a useful basis for understanding the process behavior. Tetra Pak should therefore interpret the results as guiding trends rather than exact predictions.

Overall, the study demonstrates that a structured, model based approach can support extrusion screw design and reduce reliance on trial-and-error. The developed framework provides a practical tool for guiding design decisions and contributes to increased understanding of the relationship between screw geometry and process performance.

References

[1] Tetra Pak. *Tetra Top 1000 Base CB*. Available at https://productxplorer.tetrapak.com/packages/all-packages/tetra-top-1000-base-cb-eifel-c38. Accessed May 18 , 2026. 2026.

[2] United Nations Regional Information Centre. *SDG 12: Responsible Consumption and Production*. Available at https://unric.org/en/sdg-12/. Accessed February 05 , 2026. 2026.

[3] United Nations Regional Information Centre. *SDG 9: Industry, Innovation and Infrastructure*. Available at https://unric.org/en/sdg-9/. Accessed February 05 , 2026. 2026.

[4] Design Council. *Framework for Innovation*. Available at https://www.designcouncil.org.uk/our-resources/framework-for-innovation/. Accessed April 02, 2026. 2026.

[5] M. Tang. *What Does the Screw of an Injection Molding Machine Do?* Available at https://zetarmold.com/screw-injection-molding-machine/. Accessed February 11 , 2026. 2025.

[6] M. Worgull. *Hot Embossing*. 1st. Oxford, UK: Elsevier, 2009.

[7] Tetra Pak. *Maintenance Manual: Tetra Pak® TT/3*. Internal company document. Confidential internal documentation. 2025.

[8] G. A. Campbell and M. A. Spalding. *Analyzing and Troubleshooting Single-Screw Extruders*. 2nd. Cincinnati, Ohio, USA: Hanser, 2021.

[9] Glycon. *Why Screws are Designed the Way They Are*. Available at https://glycon.com/wp-content/uploads/2019/06/pdf3.pdf. Accessed February 16 , 2026. 2019.

[10] Z. Tadmor and C. G. Gogos. *Principles of Polymer Processing*. 2nd. Hoboken, New Jersey, USA: Wiley-Interscience, 2006.

[11] Bruce A. Davis et al. *Grooved Feed Single Screw Extruders - Improving Productivity and Redusing Viscous Heating Effects*. Available at https://productxplorer.tetrapak.com/packages/all-packages/tetra-top-1000-base-cb-eifel-c38. Accessed May 18 , 2026. 2026.

[12] seawin. *Injection Molding Barrels: Material Design Guide*. Available at https://www.seawinindustrial.com/processes-technology/injection-molding-barrel-guide/. Accessed February 16 , 2026. 2025.

[13] F. Chen. *Injection Molding Screws and Barrels - Design and Tips*. Available at https://www.boyiprototyping.com/injection-molding-guide/injection-molding-screws-and-barrels/. Accessed February 16 , 2026. 2024.

[14] Autodesk. *Cross–WLF Viscosity Model — Moldflow Insight Help*. Available at https://help.autodesk.com/view/MFIA/2023/ENU/?guid=MoldflowInsight_CLC_Ref_Materials_sim_math_models_Cross_WLF_viscosity_model_html. Accessed April 07, 2026. 2023.

[15] E. Mejia et al. *Effect of Processing Techniques on the Microstructure and Mechanical Performance of High-Density Polyethylene*. Available at https://www.mdpi.com/2073-4360/13/19/3346. Accessed April 16, 2026. 2021.

[16] SIEMENS. *Simcenter STAR-CCM+ software*. Available at https://www.siemens.com/en-us/products/simcenter/fluids-thermal-simulation/star-ccm/. Accessed February 11, 2026. 2026.

[17] PTC. *Advanced 3D modeling software - the future of how you design*. Available at https://www.ptc.com/en/products/creo/parametric. Accessed February 12, 2026. 2026.

[18] SIEMENS Xcelerator Academy. *CFD Analysis: Fundamentals*. Available at https://training.plm.automation.siemens.com/mytraining/libraries.cfm?mem=LAAS80005&library=YCuNPepWq&product=XAPID525869788. Accessed March 11, 2026. 2026.

[19] LLC Minitab. *Minitab Statistical Software*. Available at https://www.minitab.com/en-us/products/minitab/. Accessed May 19, 2026. 2026.

[20] LLC Minitab. *Screening designs*. Available at https://support.minitab.com/en-us/minitab/help-and-how-to/statistical-modeling/doe/supporting-topics/factorial-and-screening-designs/screening-designs/. Accessed May 07, 2026. 2026.

[21] LLC Minitab. *Factorial and fractional factorial designs*. Available at https://support.minitab.com/en-us/minitab/help-and-how-to/statistical-modeling/doe/supporting-topics/factorial-and-screening-designs/factorial-and-fractional-factorial-designs/. Accessed May 07, 2026. 2026.

[22] LLC Minitab. *What are responce surface designs, central composite designs, and Box-Behnken designs?* Available at https://support.minitab.com/en-us/minitab/help-and-how-to/statistical-modeling/doe/supporting-topics/response-surface-designs/response-surface-central-composite-and-box-behnken-designs/#what-is-a-central-composite-design. Accessed May 07, 2026. 2026.

[23] LLC Minitab. *What is response optmization?* Available at https://support.minitab.com/en-us/minitab/help-and-

how-to/statistical-modeling/using-fitted-models/supporting-topics/response-optimization/what-is-response-optimization/. Accessed May 12, 2026. 2026.

[24] LLC Minitab. *Determining the weight in response optimization*. Available at https://support.minitab.com/en-us/minitab/help-and-how-to/statistical-modeling/using-fitted-models/supporting-topics/response-optimization/determining-the-weight/. Accessed May 12, 2026. 2026.

[25] LLC Minitab. *Composite desirability*. Available at https://support.minitab.com/en-us/minitab/help-and-how-to/statistical-modeling/using-fitted-models/how-to/response-optimizer/methods-and-formulas/composite-desirability/. Accessed May 25, 2026. 2026.

Appendix A. Work Distribution and Time Plan

A.1 Work Distribution

The work in this thesis was carried out collaboratively, where both students contributed to all major parts of the project. The distribution reflects how the effort was shared depending on the specific activities, while maintaining a joint responsibility for the overall outcome.

Table A.1: Overview of work distribution.

Work Task	Emma Frick	Amanda Mile	Others
Planning	50%	50%	0%
Literature study	50%	50%	0%
Numerical simulation	30%	30%	40%
Analytical modelling - mass flow	80%	20%	0%
Analytical modelling - power consumption	20%	80%	0%
CAD modelling & parameterization	50%	50%	0%
Design of Experiments (DOE) & response surface	50%	50%	0%
Optimization	30%	70%	0%
Framework development	70%	30%	0%
Report writing	50%	50%	0%

A.1.1 Declaration of Generative AI

Microsoft Copilot is a generative AI tool, and was used as a supporting resource during the thesis work. It assisted in improving English grammar and language quality, as well as in finding relevant scientific sources for the literature study and structuring and organizing information. All outputs were critically reviewed and validated by the authors.

A.2 Project Plan and Outcome

The initial project plan included both a numerical simulation approach and an analytical modeling approach, as illustrated in Figure A.1.

Following the decision to discontinue the simulation work and proceed with the analytical model only, a revised project plan was established, see Figure A.2. This updated plan reflects the adjusted project focus and the redistribution of activities.

The actual timeline of the project execution is presented in Figure A.3. This timeline reflects when the activities actually were carried out during the project.

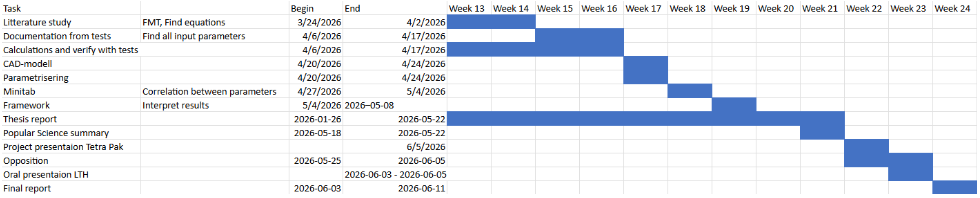

Figure A.2: The updated plan for the thesis project, only focusing on the analytical model.

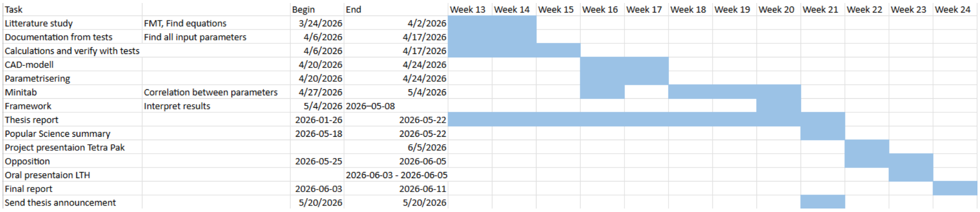

Figure A.3: The actual timeline followed during the thesis project.

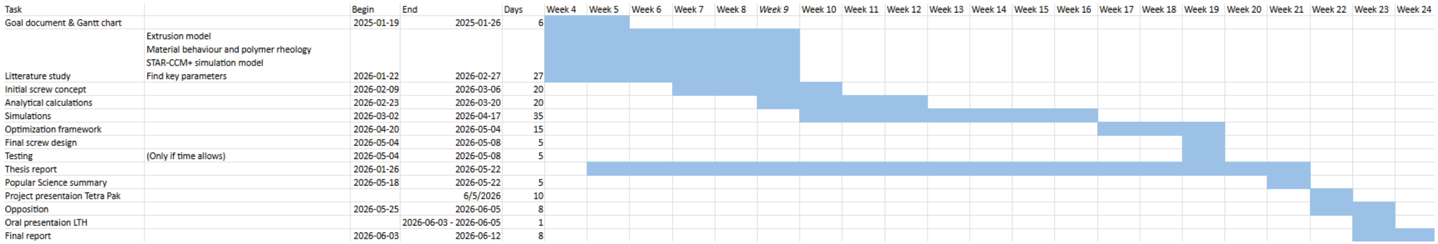

Figure A.1: The original plan for the thesis project.